Cell

A microbial transporter of the dietary antioxidant ergothioneine

Graphical abstract

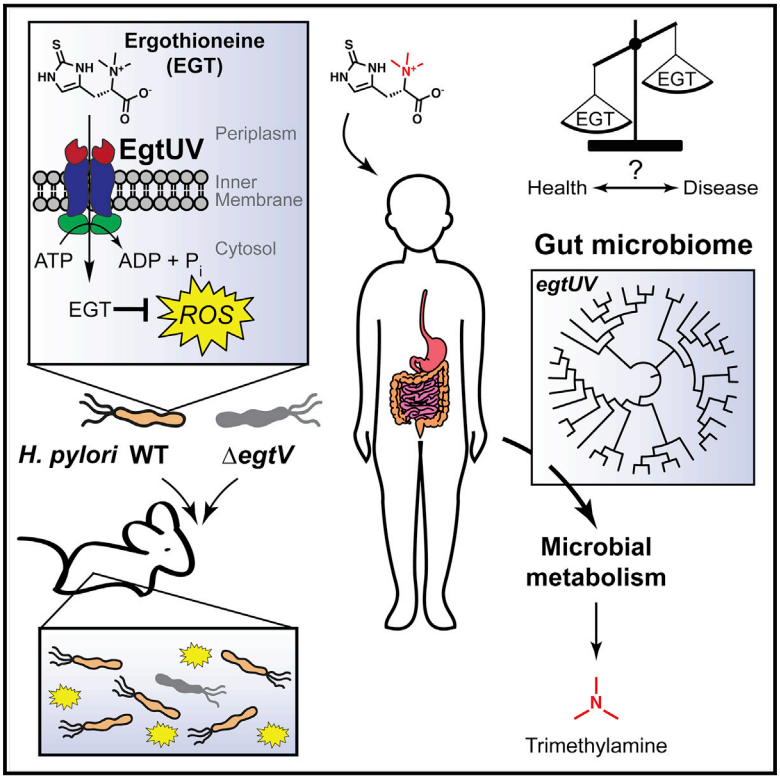

Highlights

- *Helicobacter pylori* imports the human dietary antioxidant ergothioneine (EGT)
- ABC transporter EgtUV takes up host-derived EGT and protects against bleach stress
- WT *H. pylori* outcompetes EgtUV-deficient *H. pylori* in mice
- EGT import and metabolism are widespread among human gastrointestinal microbes

Authors

Daniel G. Dumitrescu,
Elizabeth M. Gordon,
Yekaterina Kovalyova, ..., Aimee Shen,
Philip J. Kranzusch, Stavroula K. Hatzios

Correspondence

stavroula.hatzios@yale.edu

In brief

Low-molecular-weight thiols are necessary for the maintenance of intracellular redox homeostasis; however, certain clinically important microbial pathogens are not known to synthesize these antioxidants. By analyzing *H. pylori*, a microbial transporter of ergothioneine was discovered that regulates microbial redox homeostasis in the gut.

Dumitrescu et al., 2022, Cell *185*, 1–15
November 23, 2022
https://doi.org/10.1016/j.cell.2022.10.008

CellPress

Cell

CellPress

Article

A microbial transporter of the dietary antioxidant ergothioneine

Daniel G. Dumitrescu,[1,2,3] Elizabeth M. Gordon,[1,3,12] Yekaterina Kovalyova,[1,2,3,12] Anna B. Seminara,[1,3,4] Brianna Duncan-Lowey,[5,6] Emily R. Forster,[7,8] Wen Zhou,[9] Carmen J. Booth,[10] Aimee Shen,[7] Philip J. Kranzusch,[5,6,11] and Stavroula K. Hatzios[1,2,3,13,*]

[1]Department of Molecular, Cellular, and Developmental Biology, Yale University, New Haven, CT 06520, USA
[2]Department of Chemistry, Yale University, New Haven, CT 06520, USA
[3]Microbial Sciences Institute, Yale University, West Haven, CT 06516, USA
[4]Department of Microbial Pathogenesis, Yale University School of Medicine, New Haven, CT 06520, USA
[5]Department of Microbiology, Harvard Medical School, Boston, MA 02115, USA
[6]Department of Cancer Immunology and Virology, Dana-Farber Cancer Institute, Boston, MA 02115, USA
[7]Department of Molecular Biology and Microbiology, Tufts University School of Medicine, Boston, MA 02111, USA
[8]Graduate Program in Molecular Microbiology, Graduate School of Biomedical Sciences, Tufts University, Boston, MA 02111, USA
[9]Department of Immunology and Microbiology, School of Life Sciences, Southern University of Science and Technology, Shenzhen, Guangdong 518055, China
[10]Department of Comparative Medicine, Yale University School of Medicine, New Haven, CT 06520, USA
[11]Parker Institute for Cancer Immunotherapy at Dana-Farber Cancer Institute, Boston, MA 02115, USA
[12]These authors contributed equally
[13]Lead contact
*Correspondence: stavroula.hatzios@yale.edu
https://doi.org/10.1016/j.cell.2022.10.008

SUMMARY

Low-molecular-weight (LMW) thiols are small-molecule antioxidants required for the maintenance of intracellular redox homeostasis. However, many host-associated microbes, including the gastric pathogen *Helicobacter pylori*, unexpectedly lack LMW-thiol biosynthetic pathways. Using reactivity-guided metabolomics, we identified the unusual LMW thiol ergothioneine (EGT) in *H. pylori*. Dietary EGT accumulates to millimolar levels in human tissues and has been broadly implicated in mitigating disease risk. Although certain microorganisms synthesize EGT, we discovered that *H. pylori* acquires this LMW thiol from the host environment using a highly selective ATP-binding cassette transporter—EgtUV. EgtUV confers a competitive colonization advantage *in vivo* and is widely conserved in gastrointestinal microbes. Furthermore, we found that human fecal bacteria metabolize EGT, which may contribute to production of the disease-associated metabolite trimethylamine *N*-oxide. Collectively, our findings illustrate a previously unappreciated mechanism of microbial redox regulation in the gut and suggest that inter-kingdom competition for dietary EGT may broadly impact human health.

INTRODUCTION

The maintenance of redox homeostasis is essential for all cellular life. Although oxygen is necessary for aerobic metabolism, it is also the progenitor of reactive oxygen species (ROS), a family of electrophilic molecular oxidants generated by cellular respiration, immunological responses, and photo- or metallo-chemical reactions (Cabiscol et al., 2000; Sies and Jones, 2020). When excess ROS accumulate within cells, biomolecules suffer oxidative damage that can impair critical cellular processes. Consequently, the rapid remediation of oxidative stress is paramount for cell survival.

Low-molecular-weight (LMW) thiols are the principal small molecules used by all life forms to maintain intracellular redox balance (Ulrich and Jakob, 2019). LMW thiols can directly neutralize ROS and xenobiotics, regulate protein structure and function, and serve as cofactors for antioxidant and metabolic enzymes (Ulrich and Jakob, 2019; Van Laer et al., 2013). These sulfur-containing antioxidants are ubiquitous in nature. Glutathione (GSH) is the predominant LMW thiol synthesized by eukaryotes and many Gram-negative bacteria (Forman et al., 2009), but microorganisms lacking GSH typically produce functionally analogous compounds (Fairlamb et al., 1985; Gaballa et al., 2010; Newton et al., 2008; Seebeck, 2010). Defects in human GSH biosynthesis and metabolism have been implicated in debilitating metabolic disorders and neurodegenerative diseases (Ballatori et al., 2009). Similarly, the deletion of microbial LMW-thiol biosynthetic genes can attenuate bacterial survival within host environments (Krieger et al., 2000; Posada et al., 2014; Reniere et al., 2015; Saini et al., 2016), underscoring the

Please cite this article in press as: Dumitrescu et al., A microbial transporter of the dietary antioxidant ergothioneine, Cell (2022), https://doi.org/10.1016/j.cell.2022.10.008

broad importance of these protective thiols in sustaining essential cellular functions.

Although all life forms are believed to require LMW-thiol antioxidants, several classes of bacteria lack the enzymes required to synthesize them *de novo*. Many of these microbes, like the human gastric pathogen *Helicobacter pylori*, are also known to colonize animal hosts. *H. pylori* has co-evolved with humans for over 60,000 years and infects over half of the global population (Linz et al., 2007; Salama et al., 2013). *H. pylori* colonization provokes chronic inflammation and the sustained release of ROS from gastric tissues, which can contribute to the formation of peptic ulcers or cancer in a subset of infected hosts (Amieva and Peek, 2016; Butcher et al., 2017; Salama et al., 2013). How *H. pylori* maintains intracellular redox homeostasis without producing known LMW thiols, despite persistent exposure to ROS in the host, remains unresolved.

In this study, we performed a targeted metabolomic analysis to investigate potential LMW thiols in *H. pylori* and identified the unusual antioxidant ergothioneine (EGT). EGT is a thiourea derivative of histidine synthesized by few bacteria and fungi and exclusively acquired by animals and plants from exogenous sources (Cumming et al., 2018). As an abundant component of the human diet, EGT is present at high levels in gastrointestinal tissues (Tang et al., 2018). We found that *H. pylori* is unable to synthesize EGT and instead imports this compound from the host environment using a previously uncharacterized ATP-binding cassette (ABC) transporter. This transporter is widely conserved in gastrointestinal microbes, revealing a common pathway for EGT acquisition and maintenance of microbial redox homeostasis in the host.

RESULTS

H. pylori imports the antioxidant EGT

We employed a reactivity-guided metabolomics screen to identify LMW thiols in *H. pylori*, wherein bacterial cell extracts were treated with the thiol-alkylating agent monobromobimane (mBBr) (Newton and Fahey, 1995) to enable detection of mBBr-labeled metabolites by liquid chromatography-mass spectrometry (LC-MS) (Figure 1A). Consistent with the lack of known LMW-thiol biosynthetic genes in *H. pylori*, we did not detect the bimane derivatives of GSH or its functional analogs bacillithiol or mycothiol in mBBr-treated *H. pylori* extracts. However, we observed a species with a mass-to-charge ratio (*m/z*) of 420.1700 (calc. MF $C_{19}H_{26}N_5O_4S^+$), which is equivalent to the calculated *m/z* for the bimane adduct of the LMW thiol EGT (Figures 1B and 1C). This species was only present in mBBr-treated extracts (Figure 1B) and exhibited the same chromatographic properties (Figure 1D) and fragmentation pattern (Figure 1E) as an mBBr-treated EGT standard when analyzed by liquid chromatography-tandem mass spectrometry (LC-MS/MS). Together, these data support that *H. pylori* contains the LMW thiol EGT.

EGT is a sulfur-containing derivative of histidine that can scavenge potent oxidizing agents and inhibit the formation of oxygen radicals (Cheah and Halliwell, 2012). EGT exists predominantly as a thione tautomer and thus possesses a higher standard reduction potential ($E_o' = -0.06$ V) than other LMW thiols like GSH ($E_o' = -0.25$ V) (Hand and Honek, 2005). Consequently, EGT is highly stable under physiological conditions but can reduce strong oxidants such as hypochlorous acid (bleach) and peroxynitrite. Although diet-derived EGT accumulates to millimolar concentrations in animal tissues, it is only synthesized by select fungal and bacterial species (Halliwell et al., 2018). The enzymes required for EGT biosynthesis include an *S*-adenosyl methionine (SAM)-dependent methyltransferase, an iron(II)-dependent sulfoxide synthase, and a pyridoxal 5-phosphate-dependent β-lyase (Figure S1A; Bello et al., 2012; Seebeck, 2010). However, we were unable to identify orthologs of these enzymes in *H. pylori* using bioinformatic approaches. We therefore performed culture-based assays to determine whether *H. pylori* can synthesize EGT *de novo*.

To probe for biosynthesis, we supplemented broth cultures of *H. pylori* with EGT biosynthetic precursors (Figure 1F) and measured the EGT content of mBBr-treated cell extracts by LC-MS. Addition of 1 mM histidine or methionine or 0.2 mM cysteine to *H. pylori* cultures had no effect on EGT levels (Figure 1G). We also employed isotope tracing and LC-MS to determine whether *H. pylori* can synthesize isotopically labeled EGT when grown in the presence of the EGT precursor methionine-(*methyl*-^{13}C). Although we observed the expected mass shift of +1 amu for SAM, we did not detect a similar mass shift for EGT (Figures S1B–S1D). Collectively, these data suggest canonical pathways for the production of EGT are not active in *H. pylori*.

Given that *H. pylori* culture medium is enriched with animal extracts that contain high levels of EGT (Tang et al., 2018), we hypothesized that *H. pylori* may instead acquire EGT from the extracellular environment. To test this, we compared the EGT content of conditioned culture medium with that of medium alone. We observed a significant decrease in the EGT content of *H. pylori* culture supernatants relative to that of media controls (Figure 1H), suggesting that *H. pylori* can deplete EGT from the culture medium. To determine if exogenous EGT can accumulate in *H. pylori* cells, we grew *H. pylori* in medium supplemented with isotopically labeled "heavy" EGT (EGT-d^3). We observed a dose-dependent increase in the EGT-d^3 content of *H. pylori* cell extracts and a corresponding decrease in the levels of "light" EGT (Figure 1I). Altogether, these data demonstrate that *H. pylori* can import extracellular EGT.

The ABC transporter EgtUV is required for EGT uptake by *H. pylori*

We hypothesized that *H. pylori* encodes a transporter capable of translocating EGT across lipid membranes. Indeed, certain microorganisms incapable of GSH synthesis encode a transporter for its uptake (Bachhawat et al., 2013). Although mammalian cells import EGT via the sodium symporter OCTN1 (aka SLC22A4) (Gründemann et al., 2005), no OCTN1 orthologs are encoded by the *H. pylori* genome. Notably, the chemical structure of EGT resembles that of the bacterial osmolyte glycine betaine (Figure 2A). We therefore reasoned that *H. pylori* genes annotated as hypothetical betaine transporters could be responsible for EGT import. Through bioinformatic analyses, we identified two uncharacterized *H. pylori* genes encoding putative betaine transporters, *HPG27_777* and *HPG27_885*, and analyzed the EGT content of *H. pylori* strains disrupted at either

Please cite this article in press as: Dumitrescu et al., A microbial transporter of the dietary antioxidant ergothioneine, Cell (2022), https://doi.org/10.1016/j.cell.2022.10.008

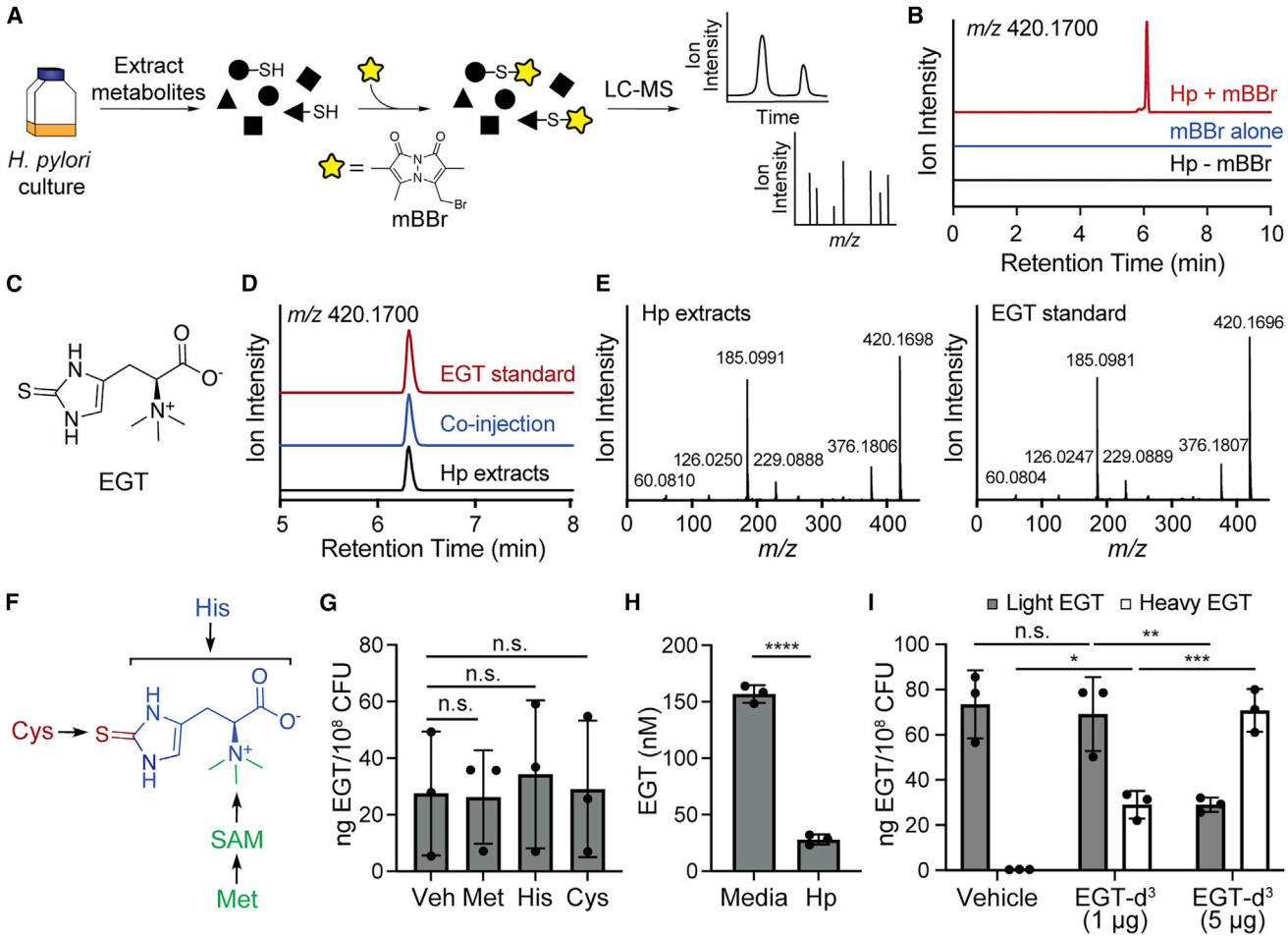

Figure 1. *H. pylori* imports the antioxidant EGT

(A) Workflow for the detection of LMW thiols in *H. pylori*.

(B) Extracted ion chromatogram (EIC) spectra (*m/z* 420.1700) of *H. pylori* (Hp) cell extracts treated with or without mBBr, and of mBBr alone.

(C) Chemical structure of EGT.

(D) EIC spectra (*m/z* 420.1700) of either *H. pylori* cell extracts or an EGT standard treated with mBBr or a 1:1 mixture of the two (co-injection).

(E) LC-MS/MS analysis of the samples from (D).

(F) His, Met, and Cys are required for EGT synthesis and are incorporated into the EGT structure as shown.

(G) *H. pylori* extracts from cultures supplemented with 1 mM His or Met, 0.2 mM Cys, or vehicle control were labeled with mBBr and analyzed by LC-MS to quantify EGT levels using a deuterated EGT standard. n.s., not significant, by one-way ANOVA.

(H) EGT content of *H. pylori* conditioned medium and of medium alone was quantified as in (G). ****$p < 0.0001$, by unpaired two-tailed t test.

(I) EGT (gray bars) and EGT-d^3 (white bars) content of *H. pylori* cell extracts from cultures supplemented with 0, 1, or 5 µg of EGT-d^3, quantified as in (G). *$p < 0.05$; **$p < 0.01$; ***$p < 0.001$; n.s., not significant, by two-way ANOVA with Tukey's multiple comparisons. Error bars represent means ± SD of biological replicates. See also Figure S1.

locus (*HPG27_777::Tn* and Δ*HPG27_885*) (Yang et al., 2019). Strikingly, *HPG27_777::Tn* cell extracts were devoid of EGT, whereas the EGT content of Δ*HPG27_885* extracts was comparable with that of wild-type (WT) cells (Figure 2B). Furthermore, genetic disruption of *HPG27_777*, but not *HPG27_885*, restored the EGT content of culture supernatants to that of media alone (Figure 2C). Together, these data suggest that *HPG27_777* is required for EGT uptake by *H. pylori*.

HPG27_777 resides in a putative two-gene operon with distinct features of a bacterial ABC transporter. *HPG27_777* is predicted to encode a MetI-like transmembrane permease fused to a C-terminal periplasmic solute-binding domain (SBD) (Figure 2D). *HPG27_778*, which lies downstream of *HPG27_777*, encodes conserved motifs characteristic of the ATPase subunits of ABC transporters (Figures 2D, S2A, and S2B; Davidson et al., 2008; Wilkens, 2015). Given that ABC transporters are multimeric complexes composed of transmembrane, solute-binding, and nucleotide-binding domains, we hypothesized that *HPG27_777* and *HPG27_778* together encode a functional EGT transporter. We generated deletion mutants of *HPG27_777* and/or *HPG27_778* in two different strains of *H. pylori*, G27MA and PMSS1, and confirmed that disruption of either gene inhibits EGT uptake (Figures 2E and S2C). Genetic complementation of *HPG27_777* and *HPG27_778* at the native

Please cite this article in press as: Dumitrescu et al., A microbial transporter of the dietary antioxidant ergothioneine, Cell (2022), https://doi.org/10.1016/j.cell.2022.10.008

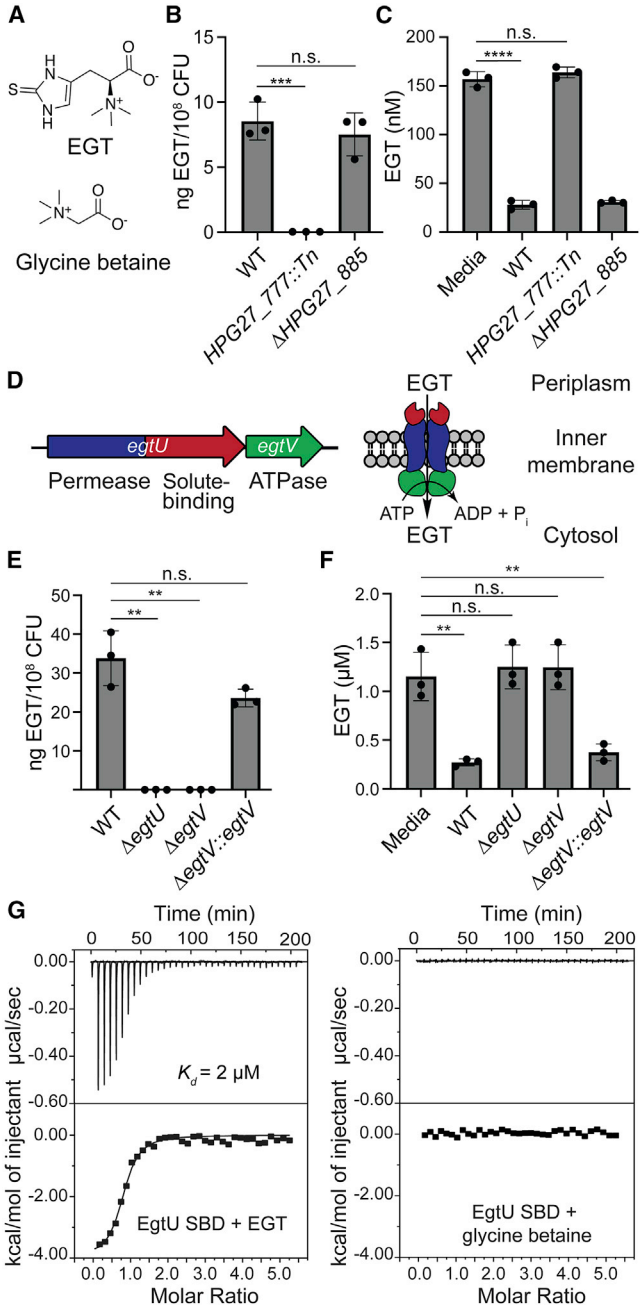

Figure 2. The ABC transporter EgtUV is required for EGT uptake by *H. pylori*

(A) Chemical structures of EGT and glycine betaine.

(B and C) EGT content of (B) cell extracts and (C) conditioned media from WT, *HPG27_777::Tn*, and Δ*HPG27_885 H. pylori* G27MA cultures was quantified by mBBr labeling and LC-MS. ***p < 0.001; ****p < 0.0001; n.s., not significant, by one-way ANOVA with Tukey's multiple comparisons. Data for WT and media controls in Figure 2C are the same as in Figure 1H.

(D) Schematic representation of transporter locus (left) and complex (right).

(E and F) EGT content of (E) *H. pylori* cell extracts and (F) conditioned medium from WT, Δ*egtU* (Δ*HPG27_777*), Δ*egtV* (Δ*HPG27_778*), and Δ*egtV::egtV* (Δ*HPG27_778::HPG27_778*) *H. pylori* G27MA cultures was quantified by mBBr labeling and LC-MS. **p < 0.01; n.s., not significant, by one-way ANOVA with Tukey's multiple comparisons.

(G) ITC analysis of EgtU SBD binding to EGT (left) or glycine betaine (right). ITC data are representative of 2–3 technical replicates. Error bars represent means ± SD of biological replicates.

See also Figures S2, S3, and Table S1.

locus, or of *HPG27_778* at a distal chromosomal site, restored the levels of cell- and media-associated EGT to those of WT *H. pylori* cultures (Figures 2E, 2F, and S2C–S2E). These findings confirm that both *HPG27_777* and *HPG27_778* (henceforth *egtU* and *egtV*, respectively) are required for EGT import by *H. pylori*.

Notably, the amount of EGT internalized by *H. pylori* (e.g., Figure 2B versus 2E) and depleted from the culture medium (e.g., Figure 2C versus 2F) varied across experiments despite identical assay conditions. We determined that the EGT content of freshly prepared culture medium decreases significantly over time (Figure S2F). Because *H. pylori* grows poorly in the absence of blood or serum, standardization of EGT levels using a chemically defined medium is not feasible. Consequently, we used fresh medium to maximize EGT uptake by *H. pylori*. Under such conditions (e.g., Figure 1I), we estimate the intracellular EGT concentration approaches ~1–2 mM (see STAR Methods), which is consistent with the typical cytosolic concentrations of other microbial LMW thiols (Fahey, 2013; Ritz and Beckwith, 2001; Van Laer et al., 2013).

To validate our genetic analyses, we expressed the EgtU SBD in *Escherichia coli* (Figure S3A) and evaluated binding of the purified protein to EGT by isothermal titration calorimetry (ITC). The EgtU SBD bound to EGT with low-micromolar affinity (K_d = 2 μM) (Figure 2G; Table S1); by contrast, we did not detect binding to the structurally similar compounds glycine betaine, choline, proline, carnitine, or histidine (Figures 2G and S3B–S3E), suggesting that EGT is the physiological ligand of EgtU. Altogether, our data support that EgtU and EgtV form an ABC importer of EGT.

H. pylori can import host-derived EGT

Given EGT is abundant in gastrointestinal tissues (Tang et al., 2018), we hypothesized that *H. pylori* may import EGT derived from gastric cells during infection. To test this, we grew human gastric adenocarcinoma (AGS) epithelial cells overnight in the presence of 1 μg/mL EGT-d^3, washed the cells to remove exogeneous EGT-d^3, and then co-cultured the AGS cells with WT, Δ*egtV*, or Δ*egtV::egtV H. pylori* G27MA (multiplicity of infection 50). After 10 h, we harvested nonadherent bacteria from the cell culture media and measured the EGT-d^3 content of the bacterial cells, AGS cells, and clarified cell culture media (Figure 3A; see STAR Methods). EGT-d^3 was only detected in AGS cells pretreated with EGT-d^3, demonstrating that AGS cells can import exogenous EGT (Figure 3B, bars 1 and 2). *H. pylori* infection did not significantly alter the EGT-d^3 content of AGS extracts (Figure 3B, bars 3–5); however, conditioned media from AGS cell cultures infected with WT or Δ*egtV::egtV H. pylori* contained ~3-fold less EGT-d^3 than media from mock-infected cultures (Figure 3C, bars 3 and 5). By contrast, the media concentration of EGT-d^3 in AGS cell cultures containing the Δ*egtV* mutant was comparable to that of AGS cells cultured in media alone (Figure 3C, bars 2 and 4). Notably, media levels of EGT-d^3 increased significantly over the 10 h incubation period even in the absence of *H. pylori* (Figure 3D), suggesting that AGS

Please cite this article in press as: Dumitrescu et al., A microbial transporter of the dietary antioxidant ergothioneine, Cell (2022), https://doi.org/10.1016/j.cell.2022.10.008

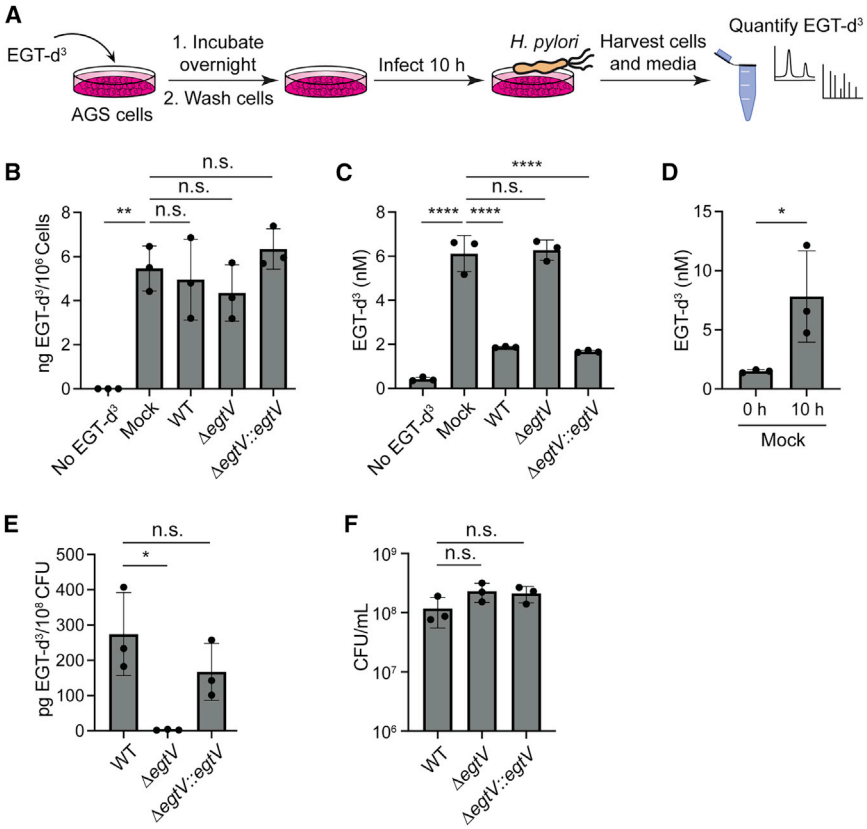

Figure 3. EgtUV can import host-derived EGT

(A) Workflow for the analysis of EGT levels in co-culture fractions.

(B–E) The EGT-d^3 content of (B) AGS cell extracts, (C) and (D) conditioned media, and (E) *H. pylori* cell extracts from AGS cells infected with WT, Δ*egtV*, or Δ*egtV::egtV H. pylori* or medium alone (mock) was quantified by mBBr labeling and LC-MS. AGS cells grown in the absence of EGT-d^3 and then mock-treated were included as a control. The EGT-d^3 content of conditioned medium from mock-treated AGS cells was quantified at t = 0 and 10 h (D). Data from the mock control in (C) appear in the 10 h time point of (D).

(F) CFU of *H. pylori* in conditioned culture media from (C). *p < 0.05; **p < 0.01; ****p < 0.0001; n.s., not significant, by one-way ANOVA with Tukey's multiple comparisons (B), (C), (E), and (F) and unpaired two-tailed t test (D). Error bars represent means ± SD of biological replicates.

cells can release intracellular EGT-d^3 into the cell culture medium. We observed corresponding trends in the bacteria harvested from these cultures: EGT-d^3 was detected in WT and Δ*egtV::egtV H. pylori*, but not in the Δ*egtV* mutant (Figure 3E), although all strains were equally viable under these conditions (Figure 3F). These data demonstrate that *H. pylori* can import EGT derived from gastric cells and that the EgtUV transporter is required for this activity.

EgtUV confers a competitive colonization advantage *in vivo*

H. pylori colonizes the gastric glands of the host, where it induces neutrophil recruitment and stimulates respiratory bursts that release ROS such as bleach and hydrogen peroxide into the infection microenvironment (Butcher et al., 2017; Fung et al., 2019; Salama et al., 2013). Bleach is the primary oxidant produced by activated neutrophils and can achieve millimolar levels in inflamed tissues (Ulfig and Leichert, 2021; Weiss, 1989). To determine if EGT import enhances *H. pylori* resistance to such ROS, we cultured WT, Δ*egtV*, and Δ*egtV::egtV H. pylori* in standard growth medium, which naturally contains EGT (Figure S2F), and compared the colony-forming units (CFUs) of each strain following exposure to 5 mM bleach or hydrogen peroxide. Bleach treatment reduced the CFU of all three strains relative to vehicle-treated controls after 15 min; however, the Δ*egtV* mutant produced ~10-fold fewer CFU than the WT and Δ*egtV::egtV* strains (Figure 4A). Lower concentrations of bleach had a subtler effect on Δ*egtV* viability, whereas 10 mM bleach completely inhibited *H. pylori* growth (Figures S4A and S4B). By contrast, hydrogen peroxide treatment did not inhibit growth of any of the strains (Figure 4B), suggesting that other mechanisms of the *H. pylori* antioxidant response (e.g., catalase production) may be sufficient to detoxify hydrogen peroxide under the tested conditions. These findings suggest that EGT uptake may selectively increase *H. pylori* resistance to the neutrophil oxidant bleach.

Bleach was recently shown to be a chemoattractant for *H. pylori* (Perkins et al., 2019). Because chemotaxis facilitates *H. pylori* colonization of the gastric glands (Howitt et al., 2011; Keilberg et al., 2016), and EgtUV enhances *H. pylori* resistance to bleach, we next assessed whether EGT import influences *H. pylori* colonization *in vivo*. Notably, EGT is present in mouse chow, gastric tissue, and digested food (Figure S4C), suggesting *H. pylori* has ample access to EGT in the gastric environment. We orally infected female C57BL/6J mice with WT, Δ*egtV*, or Δ*egtV::egtV H. pylori* or with a 1:1 mixture of the mutant and WT or complemented strains. We then quantified the *H. pylori* CFU in murine gastric tissues at either 1, 8, and 16 weeks post-infection (single infections) to evaluate colonization dynamics over time or at 2 weeks post-infection (co-infections) to evaluate competition for the gastric niche at an early time point when *H. pylori* is known to establish gland occupancy (Figure 4C; Keilberg et al., 2016). In singly colonized mice, deletion of *egtV* had no effect on *H. pylori* gastric colonization at any time point (Figure 4D). In addition, mice infected with WT, Δ*egtV*, or Δ*egtV::egtV H. pylori* for 16 weeks displayed similar gastric tissue histopathology (Figures S4D–S4H). By contrast, when we co-infected mice with a 1:1 mixture of WT and Δ*egtV H. pylori*, the WT strain exhibited a significant colonization advantage: after 2 weeks, WT *H. pylori* outcompeted the Δ*egtV* mutant by ~20-fold (Figures 4E and S4I). A similar trend was observed in

Please cite this article in press as: Dumitrescu et al., A microbial transporter of the dietary antioxidant ergothioneine, Cell (2022), https://doi.org/10.1016/j.cell.2022.10.008

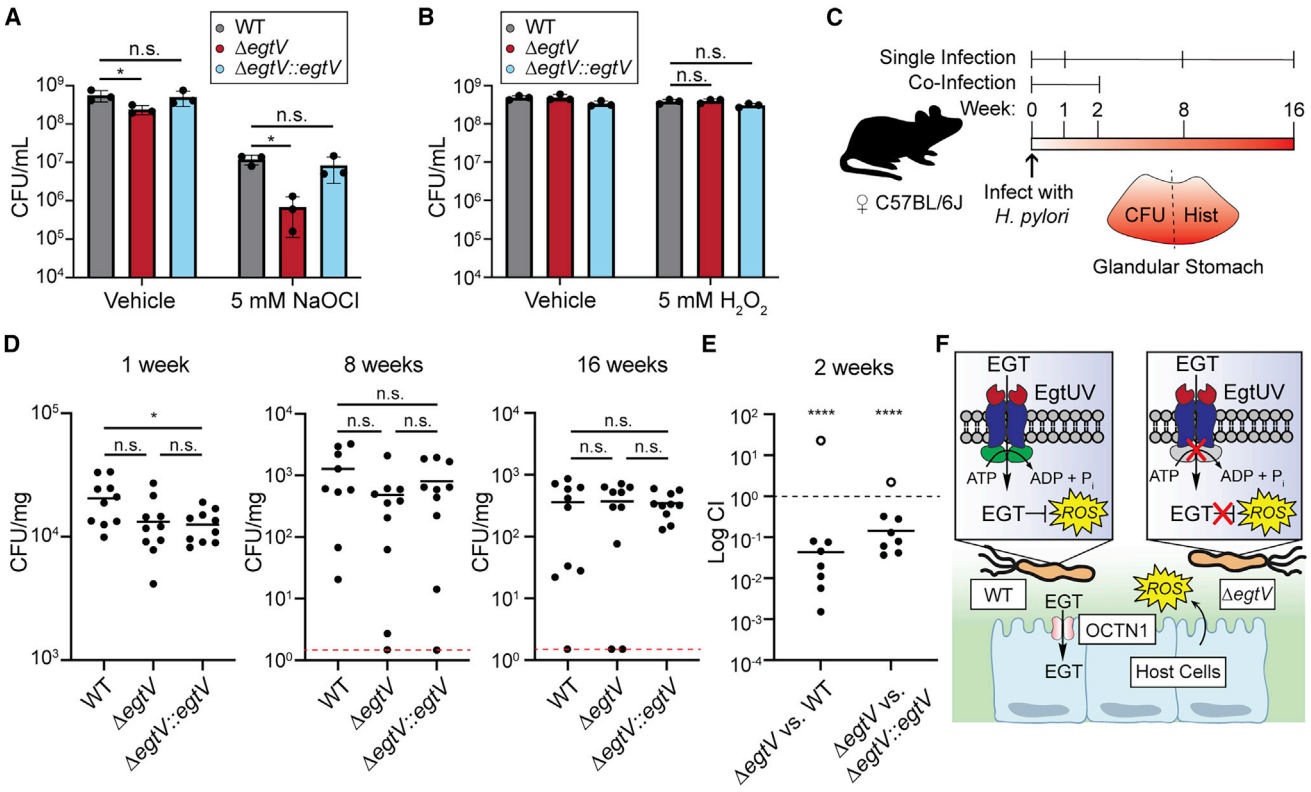

Figure 4. EgtUV confers a competitive colonization advantage *in vivo*

(A and B) CFU of WT, Δ*egtV*, and Δ*egtV::egtV H. pylori* G27MA were enumerated following treatment with (A) bleach (NaOCl; 5 mM, 15 min) or (B) hydrogen peroxide (H_2O_2; 5 mM, 3 h). *p < 0.05; n.s., not significant, by two-way ANOVA with Fisher's LSD test. Error bars represent means ± SD of biological replicates.

(C) Timeline for mouse single and co-infections with *H. pylori* PMSS1. For single infections, the stomach was divided in two for CFU enumeration and histopathology (Hist) analysis.

(D) CFU of WT, Δ*egtV*, and Δ*egtV::egtV H. pylori* in the stomachs of singly colonized mice at 1, 8, and 16 weeks post infection. N = 10 mice per condition. Horizontal bars denote the mean CFU. The limit of detection is denoted by the dashed red line. *p < 0.05; n.s., not significant, by one-way ANOVA with Tukey's multiple comparisons.

(E) Competitive indices of mice co-infected with a 1:1 mixture of either Δ*egtV* and WT or Δ*egtV* and Δ*egtV::egtV H. pylori* at 2 weeks post-infection. N = 8 mice per condition. ****p < 0.0001; competitive indices were normalized by the input ratio and compared with a hypothetical mean of 1 using a one-sample t test. Open circles denote outliers removed via Grubbs' test. Horizontal bars denote the geometric mean. All animal colonization experiments were performed twice with similar results.

(F) Working model for the functional role of *H. pylori* EgtUV *in vivo*.

See also Figures S4 and S5.

mice co-infected with Δ*egtV::egtV* and Δ*egtV H. pylori* (Figures 4E and S4J), demonstrating the functional importance of EgtV *in vivo*. Notably, WT, Δ*egtV*, and Δ*egtV::egtV H. pylori* had uniform growth kinetics when cultured individually *in vitro* (Figure S5A), but when co-cultured in a 1:1 ratio, the WT and complemented strains outcompeted the mutant strain by roughly 10-fold after 21 h (Figures S5B–S5D). Altogether, these results demonstrate that EgtUV confers a competitive colonization advantage to *H. pylori* in the gastric environment. Because gastric cells also actively import EGT, our data imply that competition for this metabolite at the host-microbe interface may influence microbial homeostasis *in vivo* (Figure 4F).

EgtUV is widely conserved in gastrointestinal microbes

We next conducted a bioinformatic analysis to survey the extent of EgtUV conservation in other microbial species. Because the substrate specificities of ABC transporters are dictated by their respective SBDs, we performed BLASTp searches for EgtUV homologs using the EgtU SBD as the query sequence in order to reduce the identification of proteins with sequence similarity to more widely conserved elements of ABC transporters. Our analysis uncovered EgtUV homologs encoded by numerous bacterial phyla, including Firmicutes, Proteobacteria, and Actinobacteria (Table S2). Putative EGT transporters were identified in many clinically important pathogens and members of the human gut microbiota (e.g., *Salmonella enterica* Typhimurium, *Clostridioides difficile*, and *Eggerthella lenta*), including the major archaeal species of the gut, *Methanobrevibacter smithii* (Figure 5A; Table S2). All identified EgtUV homologs belong to the OpuAC family of ABC transporters (Pfam), a protein family often transcriptionally and/or post-translationally regulated by oxidative, osmotic, or starvation stress (Checroun and Gutierrez, 2004;

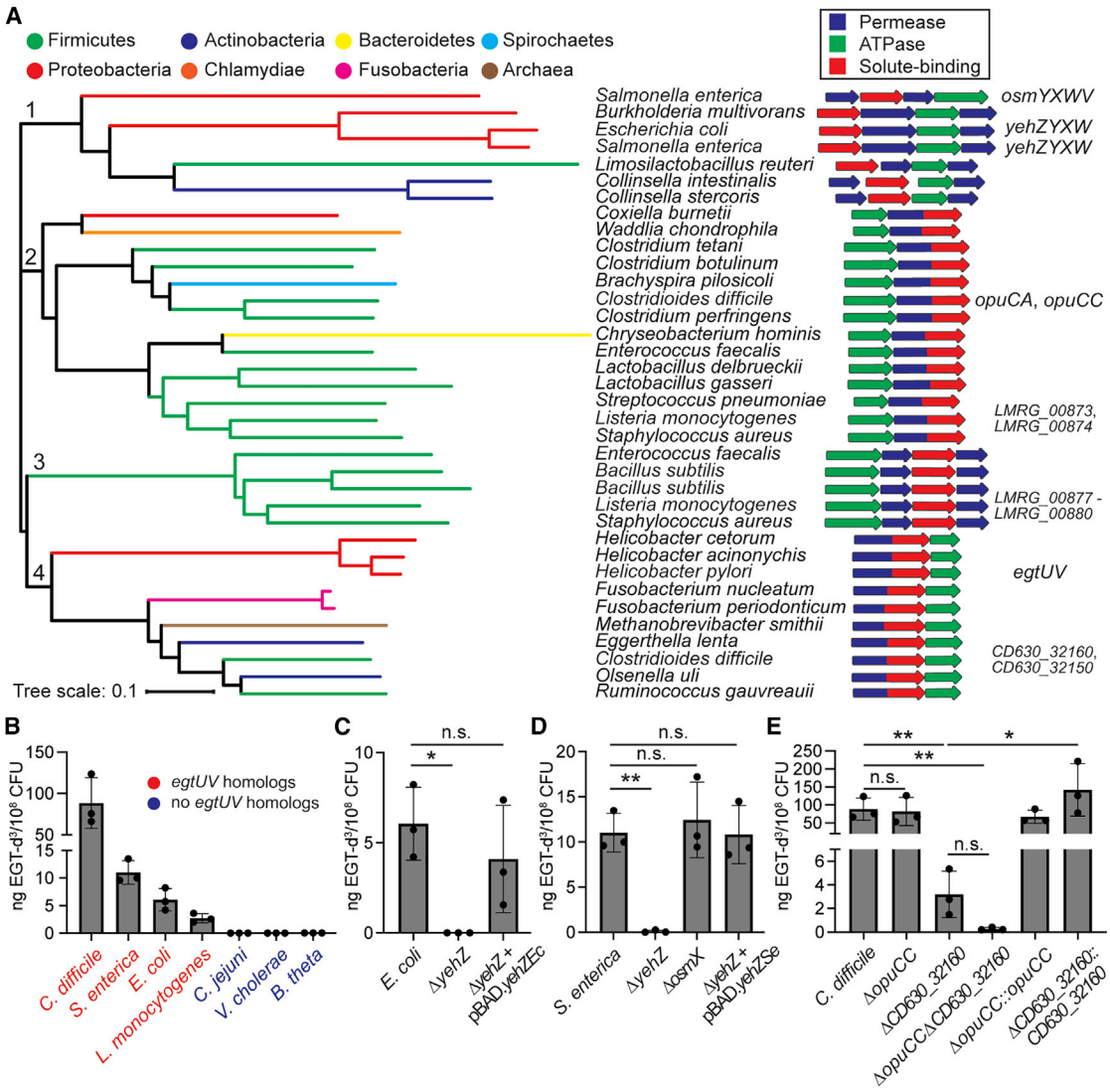

Figure 5. EgtUV is widely conserved in gastrointestinal microbes

(A) A neighbor-joining phylogenetic tree was generated using the amino-acid sequences of 35 microbial homologs of the *H. pylori* EgtU SBD (Geneious Prime). Phyla are denoted by branch color. The corresponding gene clusters are shown on the right, with permease, ATPase, and SBD subunits indicated. Four clades of differing operon structure are labeled.

(B) EGT-d^3 content of cell extracts from diverse bacterial species that either encode or lack an *egtUV* homolog. Bacteria were cultured in the presence of EGT-d^3 prior to mBBr labeling and LC-MS.

(C–E) EGT-d^3 content of cell extracts from the indicated WT, mutant, and complemented strains of (C) *E. coli*, (D) *S. enterica* Typhimurium, and (E) *C. difficile* was quantified as in (B). *$p < 0.05$; **$p < 0.01$; n.s., not significant, by one-way ANOVA with Holm-Šídák's multiple comparisons test. Error bars represent means ± SD of biological replicates.

See also Table S2.

Herrou et al., 2017; Huynh et al., 2016; Kim et al., 2013; Schuster et al., 2016). However, the physiological functions and ligands of many of these homologs are unknown (Lang et al., 2015; Michel et al., 2022).

We constructed a protein phylogenetic tree using the sequences of 35 EgtU-like SBDs from microbial species spanning diverse phyla (Figure 5A). The putative transporters clustered into four distinct clades differentiated by the genomic architectures of the transporter loci, which consisted of either 2- or 4-gene operons. Notably, the phylogenetic distribution of EgtU SBD homologs contradicts classic taxonomic relationships, suggesting *egtUV* may have been horizontally acquired.

To test whether EgtUV homology is predictive of EGT transport, we cultured bacteria that either encode or lack transporter homologs in media supplemented with EGT-d^3 and measured EGT-d^3 uptake by LC-MS. We detected EGT-d^3 in the cell extracts of all species containing *egtUV* orthologs (*C. difficile*, *S. enterica* Typhimurium, *E. coli*, and *Listeria monocytogenes*);

Please cite this article in press as: Dumitrescu et al., A microbial transporter of the dietary antioxidant ergothioneine, Cell (2022), https://doi.org/10.1016/j.cell.2022.10.008

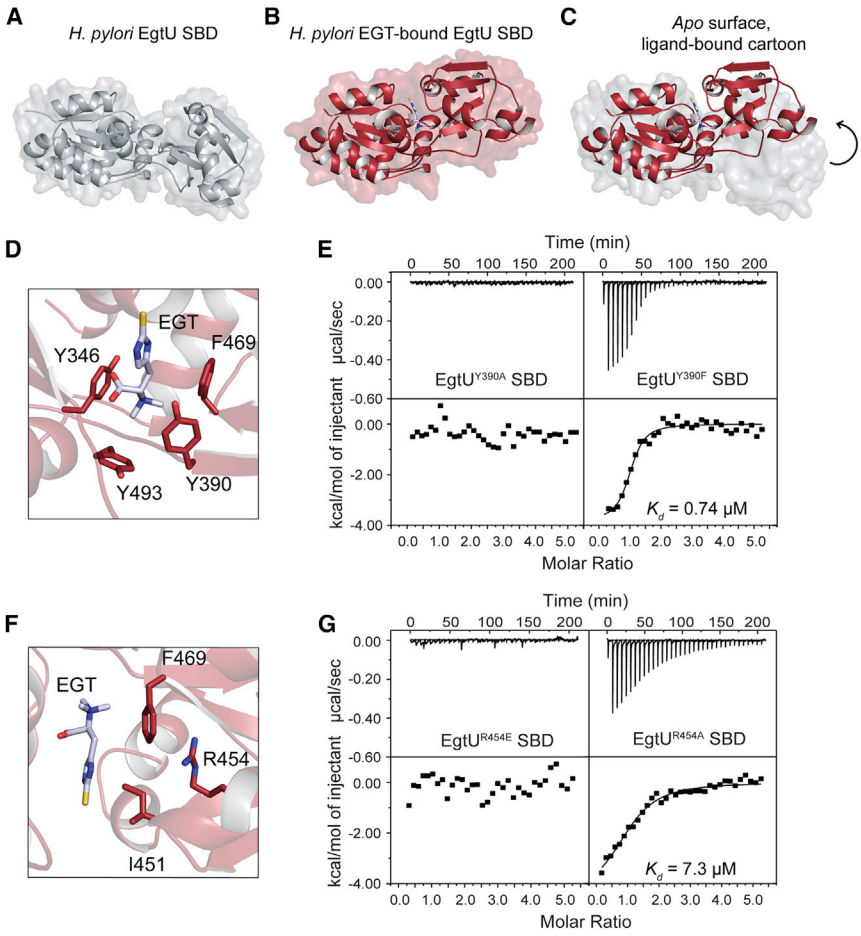

Figure 6. *H. pylori* EgtU SBD binds EGT using both conserved and unique features

(A and B) Cartoon representation of *H. pylori* EgtU crystal structure showing the two-lobed architecture in the *apo* form (A) and bound to EGT (B).

(C) Comparison of *apo* (gray surface) and EGT-bound (red cartoon) crystal structures, highlighting the domain movement upon ligand binding that closes the binding pocket around EGT.

(D and F) Zoom in of EGT-binding pocket of EgtU, showing the (D) aromatic betaine box residues surrounding EGT or (F) side chains interacting with the thioimidazole portion of EGT.

(E and G) ITC analysis of Y390 (E) or R454 (G) EgtU SBD mutants binding to EGT. K_d values are the average of the two independent experiments.

See also Figures S6, S7, and Tables S1 and S3.

however, bacteria lacking any portion of the transporter locus were devoid of EGT-d^3 (Figure 5B). Disruption of the putative SBD-encoding genes of *E. coli* and *S. enterica* (aka *yehZ*) prevented bacterial uptake of EGT-d^3, and internalization was restored by complementation of the mutant strains (Figures 5C and 5D). Similarly, deletion of the *egtU* homolog in *C. difficile* (*CD630_32160*) nearly eliminated EGT transport activity (Figure 5E). Notably, a second EgtUV-like transporter encoded by *S. enterica*—OsmYXWV (Frossard et al., 2012)—is dispensable for EGT import (Figure 5D), whereas the *C. difficile* EgtUV paralog OpuCC may contribute to EGT uptake in the absence of CD630_32160 (Figure 5E). Altogether, these data demonstrate EGT import is a widespread microbial process mediated by the conserved ABC-type transporter EgtUV.

H. pylori EgtU SBD binds EGT using both conserved and unique features

To define the mechanism of EgtU binding to EGT, we determined a 1.3 Å crystal structure of the *H. pylori* EgtU SBD and a 3.4 Å structure of the EgtU-EGT complex (Figures 6A and 6B; Table S3). Similar to other type II solute-binding proteins in ABC transporters, the EgtU SBD adopts a bi-lobed architecture with two α/β lobes connected by a central hinge (Schiefner et al., 2004a). In the ligand-bound form, the EgtU SBD lobes collapse at the central hinge region and rotate ~40° to close around EGT (Figure 6C). EGT is bound deep within the cleft between the α/β lobes (Figures 6B and S6A), with a conserved "betaine box" formed by residues Y346, Y390, F469, and Y493 at the back of the pocket that cages the EGT trimethylammonium group (Figure 6D). Betaine box motifs are conserved in other solute-binding proteins of ABC transporters that recognize ligands structurally similar to EGT including glycine betaine (Figures S6B and S6C; Schiefner et al., 2004a, 2004b). Consistent with a role for aromatic side chains in forming a hydrophobic cage, an EgtU Y390A mutation disrupted EGT binding, whereas a conservative Y390F mutation did not impede ligand recognition (Figures 6E, S6D, and S6E; Table S1). Several residues coordinate the thioimidazole moiety of EGT at the front of the pocket, including R454. Notably, a positively charged residue is conserved at this site in EGT transporter proteins YehZ of *E. coli* and *S. enterica* and CD630_32160 of *C. difficile*, but not in *E. coli* ProX or *S. enterica* OsmX (Figures 6F and S7). A charge-swap mutation of this residue, R454E, resulted in the complete loss of EGT binding, whereas an R454A mutation retained EGT binding, albeit with ~4-fold lower affinity than WT (Figures 6G, S6D, and S6E; Table S1). Together, these data confirm that EgtU functions as an EGT-specific solute-binding protein and provide a molecular basis for ligand recognition.

EGT is metabolized by human fecal bacteria

Given the widespread distribution of EgtUV in gastrointestinal microbes, we next considered whether EGT can be metabolized by human gut commensals. Dietary compounds containing quaternary ammonium groups, such as choline, glycine betaine, and carnitine, can be metabolized to trimethylamine (TMA) by gut bacteria (Rath et al., 2019). TMA is then further oxidized by monooxygenases in the liver to produce TMA *N*-oxide (TMAO), a metabolite broadly associated with cardiovascular disease

Please cite this article in press as: Dumitrescu et al., A microbial transporter of the dietary antioxidant ergothioneine, Cell (2022), https://doi.org/10.1016/j.cell.2022.10.008

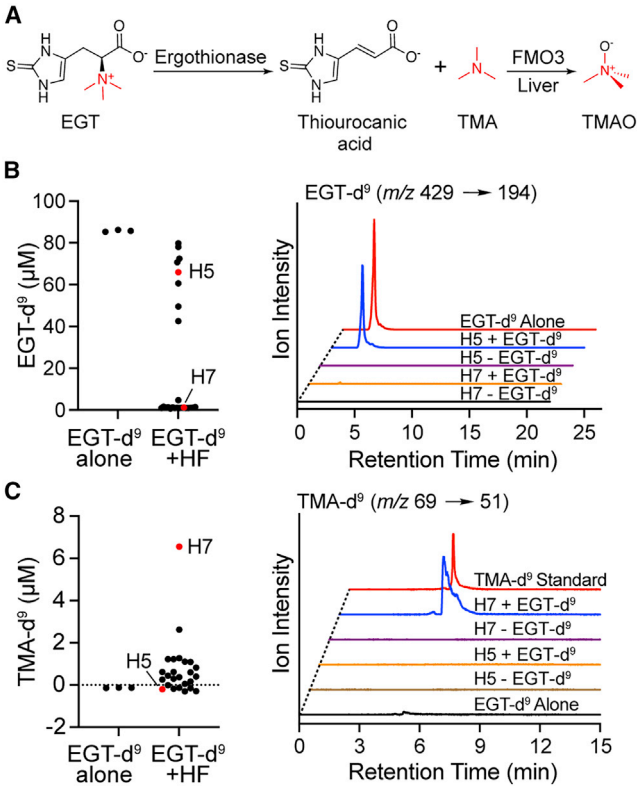

Figure 7. EGT is metabolized by human fecal bacteria

(A) The microbial enzyme ergothionase converts EGT into thiourocanic acid and trimethylamine (TMA), which can be oxidized by host enzymes to trimethylamine *N*-oxide (TMAO).

(B and C) (B) EGT-d^9 and (C) TMA-d^9 levels were quantified following anaerobic incubation of EGT-d^9 with each of 25 human fecal (HF) samples for 24 h (left). Traces of EGT-d^9 (B) and TMA-d^9 (C) fragmentation products in mixtures containing one of two representative fecal samples (H5 and H7) or EGT-d^9 and TMA-d^9 alone are shown on the right. EGT-d^9 levels in (B) were quantified via mBBr labeling and LC-MS using an EGT-d^3 internal standard. TMA-d^9 levels in (C) were quantified using the linear range of a TMA-d^9 standard curve.

(Fennema et al., 2016; Velasquez et al., 2016). Similarly, EGT can be degraded to TMA and thiourocanic acid by the enzyme ergothionase (Figure 7A; Beliaeva et al., 2021; Maurer et al., 2019; Muramatsu et al., 2013), which is encoded by several microbial species, but not *H. pylori*. However, it is unknown whether EGT can be metabolized by gut commensal bacteria or whether microbial metabolism of EGT can contribute to TMA production in the host. To address these questions, we incubated human fecal (HF) samples from 25 healthy individuals, which contained similar levels of viable and taxonomically diverse bacteria (Zimmermann et al., 2019), with 25 μg EGT-d^9 under anerobic conditions, and quantified the degradation of EGT-d^9 (Figure 7B) and its conversion to TMA-d^9 (Figure 7C) by LC-MS. Of the 25 tested samples, 17 degraded EGT-d^9 by over 90%, whereas the remaining 8 samples exhibited variable activity, degrading EGT-d^9 by 7%–50% (Figure 7B). One sample with high EGT-degrading activity (H7) also produced TMA-d^9 (Figure 7C). These results suggest EGT is catabolized by gut bacteria and that in a subset of individuals, EGT can be converted to TMA in the host. As such, EGT may not only enhance the antioxidant response of EGT-importing bacteria but also fuel the production of bioactive metabolites like TMAO that impact host physiology.

DISCUSSION

We identified a highly selective microbial transporter of the LMW thiol EGT. EGT import fortifies *H. pylori* resistance to oxidative stress and allows the pathogen to compete successfully for colonization of the gastric mucosa. Widespread distribution of the EgtUV transporter in gastrointestinal microbes reveals a previously unappreciated role for dietary EGT in regulating microbial redox biology within the host. Furthermore, cross-kingdom competition for EGT, coupled with the emerging immunomodulatory and neuroprotective activities of this metabolite *in vivo* (see below), suggest that microbial import and metabolism of EGT may broadly influence host physiology.

EGT import by *H. pylori*

Resistance to oxidative stress is a critical aspect of *H. pylori* adaptation to the host environment that underlies gastric pathology. Chronic *H. pylori* infection induces sustained inflammatory processes that can injure host tissues and potentiate cancer development. Although various antioxidant enzymes are necessary for *H. pylori* survival under oxidizing conditions (Wang et al., 2006), EGT is the only LMW thiol shown to reinforce the pathogen's antioxidant response. We found EGT import is required for *H. pylori* resistance to bleach (Figure 4A). Recent work by Guillemin and coworkers demonstrated that *H. pylori* is attracted to bleach (Perkins et al., 2019), which may facilitate persistent colonization of inflamed tissues. Indeed, *H. pylori* mutants lacking the bleach-responsive chemoreceptor TlpD exhibit reduced gland occupancy (Collins et al., 2018; Huang et al., 2017). Several chemotaxis-deficient strains with gland colonization defects are dramatically outcompeted by WT *H. pylori* in co-infected mice despite colonizing gastric tissues to similar levels as WT *H. pylori* in singly infected mice (Andermann et al., 2002; Howitt et al., 2011). As such, the increased bleach tolerance conferred by *H. pylori* import of EGT likely facilitates bacterial colonization of the glandular niche and may account for the competitive colonization advantage of EgtUV-expressing strains *in vivo* (Figure 4E).

The ability of *H. pylori* to import EGT likely reflects its long co-evolutionary history with humans. Because *H. pylori* is routinely exposed to dietary products in the gastric environment, it has a limited biosynthetic capacity and encodes multiple transport systems to internalize host metabolites (Burns and Mendz, 2001). Precisely how *H. pylori* forages EGT from the host remains unclear. EGT may be directly acquired from digested food in the stomach lumen; alternatively, *H. pylori* may appropriate EGT from gastric cells or erythrocytes. Cellular damage induced by secreted *H. pylori* proteins or local inflammation could stimulate the leakage of intracellular EGT. Alternatively, host tissues may secrete EGT via an efflux pump prior to *H. pylori* uptake. Further studies are needed to evaluate *H. pylori* import of EGT from normal gastric cells, to establish the primary EGT reservoir for *H. pylori in vivo*, and to determine whether other bacterial or

Please cite this article in press as: Dumitrescu et al., A microbial transporter of the dietary antioxidant ergothioneine, Cell (2022), https://doi.org/10.1016/j.cell.2022.10.008

host proteins are necessary for microbial acquisition of dietary EGT in the gastrointestinal tract.

Conservation of the EgtUV transporter

The EgtUV transporter is conserved in microbes from diverse phyla with wide-ranging physiological properties (Figure 5A). We speculate that the transporter locus was horizontally acquired due to the phylogenetic incongruence between the transporter genes and the microorganisms encoding them. For example, the *H. pylori* EgtU SBD shares greater amino-acid sequence similarity with homologs encoded by Fusobacteria, Firmicutes, and Actinobacteria than with homologs encoded by other Proteobacteria. Since EGT is a common component of the mammalian diet, *egtUV* may have been laterally acquired to support microbial adaptation to the host environment. Along these lines, the transporter is predominantly associated with host-adapted species of the mammalian gastrointestinal tract (Figure 5A; Table S2). Several of the transporter complexes we identified have been extensively characterized using biochemical and biophysical approaches (Du et al., 2011; Herrou et al., 2017; Lang et al., 2015; Pittelkow et al., 2011); however, in many cases, the physiological ligand(s) of the SBDs have remained elusive. The *E. coli* YehZYXW system, for example, has been classified as a low-affinity betaine transporter with binding affinities for betaine compounds in the low-millimolar range (Lang et al., 2015). Given YehZ is required for EGT import by *E. coli* and that its *H. pylori* counterpart binds to EGT with a K_d of 2 μM, we postulate that EGT is the primary substrate of YehZ and related homologs.

The assembly of bacterial ABC importers is typically orchestrated by four genes that together encode an ATPase, a permease, and a periplasmic SBD. By contrast, *H. pylori egtUV* and several of its homologs consist of just two genes, which encode an ATPase and a permease-SBD fusion protein. The *H. pylori* transporter is therefore most likely composed of a dimeric complex of EgtU and EgtV. Some of the transporter homologs we identified also contain accessory functional domains: for example, in *Staphylococcus aureus* and *L. monocytogenes*, a cystathionine β-synthase domain is attached to the EgtV C terminus and modulates ATPase activity by binding to c-di-AMP, thus regulating transporter function (Huynh et al., 2016; Schuster et al., 2016). Additional proteins that facilitate EGT uptake, such as the putative outer membrane porin that permits EGT import by Gram-negative bacteria, remain to be discovered.

Interestingly, many EgtUV homologs are present in bacteria that produce other LMW thiols. Similarly, EGT biosynthetic genes co-occur in some species that synthesize GSH or mycothiol. These findings suggest LMW-thiol biosynthesis and EGT uptake may be differentially regulated or that internalized EGT can carry out functions distinct from those of LMW thiols synthesized *de novo*. Indeed, EGT is known to regulate other important aspects of microbial physiology, such as conidial formation in fungi and energy metabolism in mycobacteria (Bello et al., 2012; Saini et al., 2016). Remarkably, *Chryseobacterium hominis*, a recently discovered Gram-negative bacterium that was isolated from human blood (Vaneechoutte et al., 2007), encodes adjacent EGT transport and biosynthetic genes, suggesting that EGT is particularly important to its life cycle. Additional studies are needed to establish the functional contributions of EGT to microbes *in vivo*, which may clarify why certain bacteria devote considerable resources to the ATP-driven import of EGT while synthesizing other LMW thiols.

Although our sequence-based search uncovered several EGT-transporting microorganisms, certain EgtUV homologs (e.g., *S. enterica* OsmYXWV) do not appear to transport EGT, underscoring the limitations of our bioinformatic approach. For certain betaine-binding proteins, like *E. coli* ProX (Schiefner et al., 2004a), it is clear that EGT cannot be accommodated by the ligand-binding site. W140 of *E. coli* ProX emerges from the front of the binding pocket (Figure S6C), where the trimethylammonium group of glycine betaine is accessible. In *H. pylori* EgtU, however, this region is occupied by the thioimidazole moiety of EGT, and the betaine-binding residues Y390 and Y493 instead reside at the back of the pocket (Figure S6C). The orientation of betaine box residues in *E. coli* ProX is consistent with this protein's ability to bind smaller betaine compounds, whereas the ligand-binding site of EgtU is configured to accommodate the larger betaine compound EGT. However, the arrangement of the betaine box residues alone is insufficient to predict whether a particular SBD can bind EGT (Figures 5D and S7). Other residues, such as EgtU R454, may play a role in determining ligand specificity. Therefore, additional studies are needed to functionally validate putative EGT transport proteins.

Competition for EGT at the host-microbe interface

Numerous studies have implicated EGT as a protective biomarker with a broad role in disease prevention. Reduced levels of EGT are associated with aging and frailty (Cheah et al., 2016; Kameda et al., 2020), neurodegenerative disorders including Parkinson's disease and dementia (Hatano et al., 2016; Teruya et al., 2021; Wu et al., 2021), and inflammatory bowel diseases like Crohn's disease (Lai et al., 2019). Similarly, treatment with EGT has been found to improve cognitive function and stimulate neuronal differentiation (Nakamichi et al., 2021) and reduce hypertension (Williamson et al., 2020) in rodent models. The mammalian EGT transporter OCTN1 is expressed in bone marrow, red blood cells, monocytes, and macrophages (Gründemann et al., 2005), and several studies have found that EGT restricts the expression of pro-inflammatory cytokines (Rahman et al., 2003; Sakrak et al., 2008), suggesting that EGT can directly modulate immune function. Single-nucleotide polymorphisms (SNPs) in the OCTN1-encoding gene *slc22a4* have been associated with Rheumatoid arthritis, Crohn's disease, and colorectal cancer (Barrett et al., 2008; Martini et al., 2012; Peltekova et al., 2004; Tokuhiro et al., 2003), although the contribution of these SNPs to Crohn's disease is debated (Huff et al., 2012). Notably, *slc22a4* expression was shown to increase over the course of murine infancy (Rakoff-Nahoum et al., 2015), a critical window of time for the maturation of the microbiota. The upregulation of *slc22a4* was dependent on functional Toll-like receptor signaling, suggesting that immune recognition of microbial signals regulates OCTN1 expression during postnatal development. Given its anti-inflammatory properties, EGT may facilitate immune adaptation to gut commensals and potentially inhibit the onset of inflammatory bowel diseases associated with dysbiosis of the intestinal flora.

Considering the widespread distribution of *egtUV* in the microbiome and the expression of OCTN1 throughout the

gastrointestinal tract (Taubert et al., 2009; Uhlén et al., 2015), our results imply that microbes compete with host cells and with each other for EGT uptake. The mammalian EGT transporter OCTN1, a member of the solute carrier (SLC) 22 protein family, contains a membrane-embedded ligand-binding site and translocates sodium ions and EGT in tandem via a mechanism of sodium symport (Volk, 2014). By contrast, the microbial EgtUV transporter utilizes an SBD to deliver EGT to a transmembrane permease domain, which then translocates EGT into the cytosol in a process driven by ATP hydrolysis. The distinct mechanisms employed by these two transporters suggest that they evolved convergently to acquire EGT and may differ in transport efficiency. Similarly, the diverse architectures of EgtUV orthologs hint at variable regulation of EGT uptake that may influence interspecies competition for this metabolite *in vivo*.

In addition to EGT transport, microbial metabolism may restrict host access to dietary EGT, which is present in both the small and large intestines (Kato et al., 2010). Indeed, our data suggest that EGT is commonly degraded by HF samples and can contribute to TMA production in the host (Figures 7B and 7C). We hypothesize that interpersonal differences in microbiome composition influence the metabolic fate of EGT. In turn, the abundance of EGT in the host diet may influence the composition of the gut microbiota, with the consumption of EGT-rich foods likely favoring microorganisms that can import or metabolize this small molecule. Notably, EGT and TMAO, which is generated via oxidation of TMA in the liver, are inversely correlated with cardiovascular health: high levels of EGT in the blood are strongly associated with reduced risk of cardiovascular disease (Smith et al., 2020), whereas high levels of TMAO are associated with elevated risk (Fennema et al., 2016; Velasquez et al., 2016). As such, the production of TMA from EGT by the gut microbiota could be detrimental to human health. EGT degradation can also generate hydrogen sulfide, which inhibits mitochondrial respiration and exacerbates inflammatory processes at high concentrations (Beliaeva et al., 2021; Rahman et al., 2020; Walsh and Giedroc, 2020). Hydrogen sulfide can also directly promote pathogen expansion during intestinal inflammation by supporting alternative respiratory pathways in the gut (Winter et al., 2010). Microbial catabolism of EGT could thus increase the risk of inflammation-associated intestinal or neurological disorders by stunting the anti-inflammatory effects of EGT *in vivo*, while also producing byproducts that negatively impact human health.

Conclusions

In summary, although genome-mining analyses have been instrumental to studies of LMW-thiol biosynthesis, our work underscores the value of reactivity-guided metabolomics for the unbiased discovery of protective thiols that may be acquired by other means. The microbial EgtUV transporter is a widely conserved mechanism of redox regulation in host-associated microbes, including the major bacterial carcinogen *H. pylori*. Interspecies competition for dietary EGT has the potential to broadly influence various aspects of host physiology, including inflammatory responses, neurobiology, and cardiovascular health, as well as the microbial ecology of the gut. Finally, because the mechanisms of EGT transport by bacterial and mammalian cells are entirely distinct, EgtU may be an attractive target for the development of broad-spectrum inhibitors that selectively block EGT import by gastrointestinal microbes in the host.

Limitations of the study

This study provides evidence of one important role for EGT in *H. pylori*—protection against the neutrophil-derived oxidant bleach. However, our findings suggest EGT constitutes a nexus that bridges the antioxidant response, cellular sulfur economy, and microbial metabolism *in vivo*. Future studies should resolve how such factors, as well as the spatial distribution of EGT in gastrointestinal tissues, influence the colonization dynamics and gland occupancy of WT versus EgtUV-deficient *H. pylori* in the stomach. Additionally, whether EgtUV directly contributes to EGT metabolism by gut bacteria is unknown. Identifying the strains responsible for degrading EGT in HF samples, and determining whether EGT catabolism contributes to disease etiology, warrants further investigation and will deepen our understanding of how EGT shapes host-microbe interactions.

STAR★METHODS

Detailed methods are provided in the online version of this paper and include the following:

- KEY RESOURCES TABLE
- RESOURCE AVAILABILITY
  - Lead contact
  - Materials availability
  - Data and code availability
- EXPERIMENTAL MODEL AND SUBJECT DETAILS
  - Bacterial strains and growth conditions
  - Mammalian cell lines and growth conditions
  - Mouse experiments
  - Human fecal samples
- METHOD DETAILS
  - Strain and plasmid construction
  - Metabolite extraction and thiol labeling
  - Liquid chromatography–mass spectrometry
  - EgtU SBD purification for ITC analysis
  - ITC analysis
  - EgtU SBD purification for crystallography
  - Crystallization and structure determination
  - Circular dichroism (CD) spectroscopy
  - Bleach and peroxide assays
  - *In vitro* growth assays
  - *H. pylori* infection of human gastric cells
  - Mouse infections
  - Measurement of EGT in mouse gastric tissue
  - Gastric histopathology
  - Bioinformatic and phylogenetic analyses
  - Human fecal EGT-d^9 metabolism assays
- QUANTIFICATION AND STATISTICAL ANALYSIS

SUPPLEMENTAL INFORMATION

Supplemental information can be found online at https://doi.org/10.1016/j.cell.2022.10.008.

ACKNOWLEDGMENTS

We thank Nina Salama (Fred Hutchinson Cancer Research Center) for *H. pylori* mutant strains and technical guidance; Jason Crawford, Jhe-Hao Li, Terence Wu (Yale West Campus Analytical Core), and Ewa Folta-Stogniew (Yale Biophysics Resource Keck Laboratory) for technical assistance and Andrew Goodman, Manuel Amieva, Eduardo Groisman, Christine Jacobs-Wagner, and Jorge Galan for bacterial strains. We are grateful to the Hatzios lab, Andrew Goodman, and Christine Jacobs-Wagner for comments on the manuscript. This work was supported by National Institutes of Health (NIH) Predoctoral training grant T32 GM067543 to D.G.D., E.M.G., and Y.K.; a Gruber Science Fellowship to E.M.G.; a Herchel Smith Graduate Fellowship to B.D.-L.; a Charles A. King Trust Postdoctoral Fellowship to W.Z.; grants from the Pew Biomedical Scholars program, a Burroughs Wellcome Investigators in the Pathogenesis of Disease Award, and the Parker Institute for Cancer Immunotherapy to P.J.K.; a Burroughs Wellcome Investigators in the Pathogenesis of Disease Award and NIAID R01 AI22232 to A.S.; and NIH R35 GM137952 to S.K.H.

AUTHOR CONTRIBUTIONS

D.G.D. and S.K.H. developed the concept for the study. All authors contributed to the design of methodology. D.G.D., E.M.G., Y.K., A.B.S., B.D.-L., E.R.F., W.Z., and C.J.B. carried out formal analysis of the data. D.G.D., E.M.G., Y.K., A.B.S., B.D.-L., E.R.F., W.Z., and C.J.B. undertook the investigation. D.G.D. and S.K.H. wrote the original draft of the manuscript. All authors reviewed and edited the manuscript. D.G.D., E.M.G., A.B.S., B.D.-L., and S.K.H. visualized the data. S.K.H. supervised the project. A.S., P.J.K., and S.K.H. oversaw administration of the project. A.S., P.J.K., and S.K.H. acquired funding for the work.

DECLARATION OF INTERESTS

A.S. is a paid consultant of LIV Process.

INCLUSION AND DIVERSITY

We support inclusive, diverse, and equitable conduct of research.

Received: April 25, 2022
Revised: August 16, 2022
Accepted: October 7, 2022
Published: November 7, 2022

SUPPORTING CITATIONS

The following references appear in the supplemental information: Amieva et al. (2003); Arnold et al. (2011); Baba et al. (2006); Guzman et al. (1995); Mandlik et al. (2011); Porwollik et al. (2014); Wollert et al. (2007).

REFERENCES

Adams, P.D., Afonine, P.V., Bunkóczi, G., Chen, V.B., Davis, I.W., Echols, N., Headd, J.J., Hung, L.W., Kapral, G.J., Grosse-Kunstleve, R.W., et al. (2010). Phenix: a comprehensive Python-based system for macromolecular structure solution. Acta Crystallogr. D Biol. Crystallogr. *66*, 213–221.

Amieva, M., and Peek, R.M., Jr. (2016). Pathobiology of *Helicobacter pylori*-induced gastric cancer. Gastroenterology *150*, 64–78.

Amieva, M.R., Vogelmann, R., Covacci, A., Tompkins, L.S., Nelson, W.J., and Falkow, S. (2003). Disruption of the epithelial apical-junctional complex by *Helicobacter pylori* CagA. Science *300*, 1430–1434.

Andermann, T.M., Chen, Y.T., and Ottemann, K.M. (2002). Two predicted chemoreceptors of *Helicobacter pylori* promote stomach infection. Infect. Immun. *70*, 5877–5881.

Arnold, I.C., Lee, J.Y., Amieva, M.R., Roers, A., Flavell, R.A., Sparwasser, T., and Müller, A. (2011). Tolerance rather than immunity protects from *Helicobacter pylori*-induced gastric preneoplasia. Gastroenterology *140*, 199–209.

Baba, T., Ara, T., Hasegawa, M., Takai, Y., Okumura, Y., Baba, M., Datsenko, K.A., Tomita, M., Wanner, B.L., and Mori, H. (2006). Construction of *Escherichia coli* K-12 in-frame, single-gene knockout mutants: the Keio collection. Mol. Syst. Biol. *2*, 2006.0008.

Bachhawat, A.K., Thakur, A., Kaur, J., and Zulkifli, M. (2013). Glutathione transporters. Biochim. Biophys. Acta *1830*, 3154–3164.

Ballatori, N., Krance, S.M., Notenboom, S., Shi, S., Tieu, K., and Hammond, C.L. (2009). Glutathione dysregulation and the etiology and progression of human diseases. Biol. Chem. *390*, 191–214.

Baltrus, D.A., Amieva, M.R., Covacci, A., Lowe, T.M., Merrell, D.S., Ottemann, K.M., Stein, M., Salama, N.R., and Guillemin, K. (2009). The complete genome sequence of *Helicobacter pylori* strain G27. J. Bacteriol. *191*, 447–448.

Barrett, J.C., Hansoul, S., Nicolae, D.L., Cho, J.H., Duerr, R.H., Rioux, J.D., Brant, S.R., Silverberg, M.S., Taylor, K.D., Barmada, M.M., et al. (2008). Genome-wide association defines more than 30 distinct susceptibility loci for Crohn's disease. Nat. Genet. *40*, 955–962.

Beliaeva, M.A., Leisinger, F., and Seebeck, F.P. (2021). *In vitro* Reconstitution of a Five-Step Pathway for Bacterial Ergothioneine Catabolism. ACS Chem. Biol. *16*, 397–403.

Bello, M.H., Barrera-Perez, V., Morin, D., and Epstein, L. (2012). The *Neurospora crassa* mutant *NcΔEgt-1* identifies an ergothioneine biosynthetic gene and demonstrates that ergothioneine enhances conidial survival and protects against peroxide toxicity during conidial germination. Fungal Genet. Biol. *49*, 160–172.

Burns, B.P., and Mendz, G.L. (2001). Metabolite transport. In *Helicobacter pylori*: physiology and genetics, H.L.T. Mobley, G.L. Mendz, and S.L. Hazell, eds. (ASM Press).

Butcher, L.D., den Hartog, G., Ernst, P.B., and Crowe, S.E. (2017). Oxidative stress resulting from *Helicobacter pylori* infection contributes to gastric carcinogenesis. Cell. Mol. Gastroenterol. Hepatol. *3*, 316–322.

Cabiscol, E., Tamarit, J., and Ros, J. (2000). Oxidative stress in bacteria and protein damage by reactive oxygen species. Int. Microbiol. *3*, 3–8.

Cheah, I.K., Feng, L., Tang, R.M.Y., Lim, K.H.C., and Halliwell, B. (2016). Ergothioneine levels in an elderly population decrease with age and incidence of cognitive decline; a risk factor for neurodegeneration? Biochem. Biophys. Res. Commun. *478*, 162–167.

Cheah, I.K., and Halliwell, B. (2012). Ergothioneine; antioxidant potential, physiological function and role in disease. Biochim. Biophys. Acta *1822*, 784–793.

Checroun, C., and Gutierrez, C. (2004). Sigma(s)-dependent regulation of *yehZYXW*, which encodes a putative osmoprotectant ABC transporter of *Escherichia coli*. FEMS Microbiol. Lett. *236*, 221–226.

Chen, V.B., Arendall, W.B., 3rd, Headd, J.J., Keedy, D.A., Immormino, R.M., Kapral, G.J., Murray, L.W., Richardson, J.S., and Richardson, D.C. (2010). MolProbity: all-atom structure validation for macromolecular crystallography. Acta Crystallogr. D Biol. Crystallogr. *66*, 12–21.

Collins, K.D., Hu, S., Grasberger, H., Kao, J.Y., and Ottemann, K.M. (2018). Chemotaxis allows bacteria to overcome host-generated reactive oxygen species that constrain gland colonization. Infect. Immun. *86*, e00878-17.

Cumming, B.M., Chinta, K.C., Reddy, V.P., and Steyn, A.J.C. (2018). Role of ergothioneine in microbial physiology and pathogenesis. Antioxid. Redox Signal. *28*, 431–444.

Davidson, A.L., Dassa, E., Orelle, C., and Chen, J. (2008). Structure, function, and evolution of bacterial ATP-binding cassette systems. Microbiol. Mol. Biol. Rev. *72*, 317–364.

Donahue, J.P., Israel, D.A., Peek, R.M., Blaser, M.J., and Miller, G.G. (2000). Overcoming the restriction barrier to plasmid transformation of *Helicobacter pylori*. Mol. Microbiol. *37*, 1066–1074.

Donnelly, M.L., Li, W., Li, Y.Q., Hinkel, L., Setlow, P., and Shen, A. (2017). A *Clostridium difficile*-specific, gel-forming protein required for optimal spore germination. mBio *8*, e02085–e02016.

Du, Y., Shi, W.W., He, Y.X., Yang, Y.H., Zhou, C.Z., and Chen, Y. (2011). Structures of the substrate-binding protein provide insights into the multiple compatible solute binding specificities of the *Bacillus subtilis* ABC transporter OpuC. Biochem. J. *436*, 283–289.

Emsley, P., and Cowtan, K. (2004). Coot: model-building tools for molecular graphics. Acta Crystallogr. D Biol. Crystallogr. *60*, 2126–2132.

Fahey, R.C. (2013). Glutathione analogs in prokaryotes. Biochim. Biophys. Acta *1830*, 3182–3198.

Fairlamb, A.H., Blackburn, P., Ulrich, P., Chait, B.T., and Cerami, A. (1985). Trypanothione: a novel bis(glutathionyl)spermidine cofactor for glutathione reductase in trypanosomatids. Science *227*, 1485–1487.

Fennema, D., Phillips, I.R., and Shephard, E.A. (2016). Trimethylamine and trimethylamine *N*-oxide, a Flavin-containing Monooxygenase 3 (FMO3)-mediated host-microbiome metabolic axis implicated in health and disease. Drug Metab. Dispos. *44*, 1839–1850.

Forman, H.J., Zhang, H., and Rinna, A. (2009). Glutathione: overview of its protective roles, measurement, and biosynthesis. Mol. Aspects Med. *30*, 1–12.

Frossard, S.M., Khan, A.A., Warrick, E.C., Gately, J.M., Hanson, A.D., Oldham, M.L., Sanders, D.A., and Csonka, L.N. (2012). Identification of a third osmoprotectant transport system, the OsmU system, in *Salmonella enterica*. J. Bacteriol. *194*, 3861–3871.

Fung, C., Tan, S., Nakajima, M., Skoog, E.C., Camarillo-Guerrero, L.F., Klein, J.A., Lawley, T.D., Solnick, J.V., Fukami, T., and Amieva, M.R. (2019). High-resolution mapping reveals that microniches in the gastric glands control *Helicobacter pylori* colonization of the stomach. PLoS Biol. *17*, e3000231.

Gaballa, A., Newton, G.L., Antelmann, H., Parsonage, D., Upton, H., Rawat, M., Claiborne, A., Fahey, R.C., and Helmann, J.D. (2010). Biosynthesis and functions of bacillithiol, a major low-molecular-weight thiol in Bacilli. Proc. Natl. Acad. Sci. USA *107*, 6482–6486.

Gibson, D.G., Young, L., Chuang, R.-Y., Venter, J.C., Hutchison, C.A., and Smith, H.O. (2009). Enzymatic assembly of DNA molecules up to several hundred kilobases. Nat. Methods *6*, 343–345.

Goodman, A.L., Kallstrom, G., Faith, J.J., Reyes, A., Moore, A., Dantas, G., and Gordon, J.I. (2011). Extensive personal human gut microbiota culture collections characterized and manipulated in gnotobiotic mice. Proc. Natl. Acad. Sci. USA *108*, 6252–6257.

Greenfield, N.J. (2006). Using circular dichroism spectra to estimate protein secondary structure. Nat. Protoc. *1*, 2876–2890.

Gründemann, D., Harlfinger, S., Golz, S., Geerts, A., Lazar, A., Berkels, R., Jung, N., Rubbert, A., and Schömig, E. (2005). Discovery of the ergothioneine transporter. Proc. Natl. Acad. Sci. USA *102*, 5256–5261.

Guzman, L.M., Belin, D., Carson, M.J., and Beckwith, J. (1995). Tight regulation, modulation, and high-level expression by vectors containing the arabinose PBAD promoter. J. Bacteriol. *177*, 4121–4130.

Halliwell, B., Cheah, I.K., and Tang, R.M.Y. (2018). Ergothioneine – a diet-derived antioxidant with therapeutic potential. FEBS Lett. *592*, 3357–3366.

Hand, C.E., and Honek, J.F. (2005). Biological chemistry of naturally occurring thiols of microbial and marine origin. J. Nat. Prod. *68*, 293–308.

Hatano, T., Saiki, S., Okuzumi, A., Mohney, R.P., and Hattori, N. (2016). Identification of novel biomarkers for Parkinson's disease by metabolomic technologies. J. Neurol. Neurosurg. Psychiatry *87*, 295–301.

Herrou, J., Willett, J.W., Czyż, D.M., Babnigg, G., Kim, Y., and Crosson, S. (2017). Conserved ABC transport system regulated by the general stress response pathways of *Alpha*- and *Gammaproteobacteria*. J. Bacteriol. *199*, e00746-16.

Howitt, M.R., Lee, J.Y., Lertsethtakarn, P., Vogelmann, R., Joubert, L.M., Ottemann, K.M., and Amieva, M.R. (2011). ChePep controls *Helicobacter pylori* infection of the gastric glands and chemotaxis in the *Epsilonproteobacteria*. mBio *2*, e00098–e00011.

Huang, J.Y., Goers Sweeney, E., Guillemin, K., and Amieva, M.R. (2017). Multiple acid sensors control *Helicobacter pylori* colonization of the stomach. PLoS Pathog. *13*, e1006118.

Huff, C.D., Witherspoon, D.J., Zhang, Y., Gatenbee, C., Denson, L.A., Kugathasan, S., Hakonarson, H., Whiting, A., Davis, C.T., Wu, W., et al. (2012). Crohn's disease and genetic hitchhiking at IBD5. Mol. Biol. Evol. *29*, 101–111.

Huynh, T.N., Choi, P.H., Sureka, K., Ledvina, H.E., Campillo, J., Tong, L., and Woodward, J.J. (2016). Cyclic di-AMP targets the cystathionine beta-synthase domain of the osmolyte transporter OpuC. Mol. Microbiol. *102*, 233–243.

Jarvik, T., Smillie, C., Groisman, E.A., and Ochman, H. (2010). Short-term signatures of evolutionary change in the *Salmonella enterica* serovar Typhimurium 14028 genome. J. Bacteriol. *192*, 560–567.

Kabsch, W. (2010). Integration, scaling, space-group assignment and post-refinement. Acta Crystallogr. D Biol. Crystallogr. *66*, 133–144.

Kameda, M., Teruya, T., Yanagida, M., and Kondoh, H. (2020). Frailty markers comprise blood metabolites involved in antioxidation, cognition, and mobility. Proc. Natl. Acad. Sci. USA *117*, 9483–9489.

Karasawa, T., Ikoma, S., Yamakawa, K., and Nakamura, S. (1995). A defined growth medium for *Clostridium difficile*. Microbiology *141*, 371–375.

Karplus, P.A., and Diederichs, K. (2012). Linking crystallographic model and data quality. Science *336*, 1030–1033.

Kato, Y., Kubo, Y., Iwata, D., Kato, S., Sudo, T., Sugiura, T., Kagaya, T., Wakayama, T., Hirayama, A., Sugimoto, M., et al. (2010). Gene knockout and metabolome analysis of carnitine/organic cation transporter OCTN1. Pharm. Res. *27*, 832–840.

Keilberg, D., Zavros, Y., Shepherd, B., Salama, N.R., and Ottemann, K.M. (2016). Spatial and temporal shifts in bacterial biogeography and gland occupation during the development of a chronic infection. mBio *7*, e01705-16.

Kim, S.I., Ryu, S., and Yoon, H. (2013). Roles of YehZ, a putative osmoprotectant transporter, in tempering growth of *Salmonella enterica* serovar Typhimurium. J. Microbiol. Biotechnol. *23*, 1560–1568.

Krieger, S., Schwarz, W., Ariyanayagam, M.R., Fairlamb, A.H., Krauth-Siegel, R.L., and Clayton, C. (2000). Trypanosomes lacking trypanothione reductase are avirulent and show increased sensitivity to oxidative stress. Mol. Microbiol. *35*, 542–552.

Lai, Y., Xue, J., Liu, C.W., Gao, B., Chi, L., Tu, P., Lu, K., and Ru, H. (2019). Serum metabolomics identifies altered bioenergetics, signaling cascades in parallel with exposome markers in Crohn's disease. Molecules *24*, 449.

Lang, S., Cressatti, M., Mendoza, K.E., Coumoundouros, C.N., Plater, S.M., Culham, D.E., Kimber, M.S., and Wood, J.M. (2015). YehZYXW of *Escherichia coli* is a low-affinity, non-osmoregulatory betaine-specific ABC transporter. Biochemistry *54*, 5735–5747.

Linz, B., Balloux, F., Moodley, Y., Manica, A., Liu, H., Roumagnac, P., Falush, D., Stamer, C., Prugnolle, F., van der Merwe, S.W., et al. (2007). An African origin for the intimate association between humans and *Helicobacter pylori*. Nature *445*, 915–918.

Mandlik, A., Livny, J., Robins, W.P., Ritchie, J.M., Mekalanos, J.J., and Waldor, M.K. (2011). RNA-Seq-based monitoring of infection-linked changes in *Vibrio cholerae* gene expression. Cell Host Microbe *10*, 165–174.

Martini, M., Ferrara, A.M., Giachelia, M., Panieri, E., Siminovitch, K., Galeotti, T., Larocca, L.M., and Pani, G. (2012). Association of the OCTN1/1672T variant with increased risk for colorectal cancer in young individuals and ulcerative colitis patients. Inflam. Bowel Dis. *18*, 439–448.

Maurer, A., Leisinger, F., Lim, D., and Seebeck, F.P. (2019). Structure and mechanism of ergothionase from *Treponema denticola*. Chemistry *25*, 10298–10303.

Michel, A.M., Borrero-de Acuña, J.M., Molinari, G., Ünal, C.M., Will, S., Derksen, E., Barthels, S., Bartram, W., Schrader, M., Rohde, M., et al. (2022). Cellular adaptation of *Clostridioides difficile* to high salinity encompasses a compatible solute-responsive change in cell morphology. Environ. Microbiol. *24*, 1499–1517.

Montgomery, R.R., Booth, C.J., Wang, X., Blaho, V.A., Malawista, S.E., and Brown, C.R. (2007). Recruitment of macrophages and polymorphonuclear leukocytes in Lyme carditis. Infect. Immun. *75*, 613–620.

Muramatsu, H., Matsuo, H., Okada, N., Ueda, M., Yamamoto, H., Kato, S., and Nagata, S. (2013). Characterization of ergothionase from *Burkholderia*

sp. HME13 and its application to enzymatic quantification of ergothioneine. Appl. Microbiol. Biotechnol. *97*, 5389–5400.

Nakamichi, N., Nakao, S., Nishiyama, M., Takeda, Y., Ishimoto, T., Masuo, Y., Matsumoto, S., Suzuki, M., and Kato, Y. (2021). Oral administration of the food-derived hydrophilic antioxidant ergothioneine enhances object recognition memory in mice. Curr. Mol. Pharmacol. *14*, 220–233.

Newton, G.L., Buchmeier, N., and Fahey, R.C. (2008). Biosynthesis and functions of mycothiol, the unique protective thiol of *Actinobacteria*. Microbiol. Mol. Biol. Rev. *72*, 471–494.

Newton, G.L., and Fahey, R.C. (1995). Determination of biothiols by bromobimane labeling and high-performance liquid chromatography. Methods Enzymol. *251*, 148–166.

Ng, Y.K., Ehsaan, M., Philip, S., Collery, M.M., Janoir, C., Collignon, A., Cartman, S.T., and Minton, N.P. (2013). Expanding the repertoire of gene tools for precise manipulation of the *Clostridium difficile* genome: allelic exchange using *pyrE* alleles. PLoS One *8*, e56051.

O'Connor, W., Jr., Kamanaka, M., Booth, C.J., Town, T., Nakae, S., Iwakura, Y., Kolls, J.K., and Flavell, R.A. (2009). A protective function for interleukin 17A in T cell-mediated intestinal inflammation. Nat. Immunol. *10*, 603–609.

Pei, J., Kim, B.H., and Grishin, N.V. (2008). PROMALS3D: a tool for multiple protein sequence and structure alignments. Nucleic Acids Res. *36*, 2295–2300.

Peltekova, V.D., Wintle, R.F., Rubin, L.A., Amos, C.I., Huang, Q., Gu, X., Newman, B., Van Oene, M., Cescon, D., Greenberg, G., et al. (2004). Functional variants of OCTN cation transporter genes are associated with Crohn disease. Nat. Genet. *36*, 471–475.

Perkins, A., Tudorica, D.A., Amieva, M.R., Remington, S.J., and Guillemin, K. (2019). *Helicobacter pylori* senses bleach (HOCl) as a chemoattractant using a cytosolic chemoreceptor. PLoS Biol. *17*, e3000395.

Pittelkow, M., Tschapek, B., Smits, S.H., Schmitt, L., and Bremer, E. (2011). The crystal structure of the substrate-binding protein OpuBC from *Bacillus subtilis* in complex with choline. J. Mol. Biol. *411*, 53–67.

Porwollik, S., Santiviago, C.A., Cheng, P., Long, F., Desai, P., Fredlund, J., Srikumar, S., Silva, C.A., Chu, W., Chen, X., et al. (2014). Defined single-gene and multi-gene deletion mutant collections in *Salmonella enterica* sv Typhimurium. PLoS One *9*, e99820.

Posada, A.C., Kolar, S.L., Dusi, R.G., Francois, P., Roberts, A.A., Hamilton, C.J., Liu, G.Y., and Cheung, A. (2014). Importance of bacillithiol in the oxidative stress response of *Staphylococcus aureus*. Infect. Immun. *82*, 316–332.

Rahman, I., Gilmour, P.S., Jimenez, L.A., Biswas, S.K., Antonicelli, F., and Aruoma, O.I. (2003). Ergothioneine inhibits oxidative stress- and TNF-alpha-induced NF-kappa B activation and interleukin-8 release in alveolar epithelial cells. Biochem. Biophys. Res. Commun. *302*, 860–864.

Rahman, M.A., Glasgow, J.N., Nadeem, S., Reddy, V.P., Sevalkar, R.R., Lancaster, J.R., Jr., and Steyn, A.J.C. (2020). The role of host-generated H_2S in microbial pathogenesis: new perspectives on tuberculosis. Front. Cell. Infect. Microbiol. *10*, 586923.

Rakoff-Nahoum, S., Kong, Y., Kleinstein, S.H., Subramanian, S., Ahern, P.P., Gordon, J.I., and Medzhitov, R. (2015). Analysis of gene-environment interactions in postnatal development of the mammalian intestine. Proc. Natl. Acad. Sci. USA *112*, 1929–1936.

Rath, S., Rud, T., Pieper, D.H., and Vital, M. (2019). Potential TMA-producing bacteria are ubiquitously found in Mammalia. Front. Microbiol. *10*, 2966.

Reniere, M.L., Whiteley, A.T., Hamilton, K.L., John, S.M., Lauer, P., Brennan, R.G., and Portnoy, D.A. (2015). Glutathione activates virulence gene expression of an intracellular pathogen. Nature *517*, 170–173.

Ritz, D., and Beckwith, J. (2001). Roles of thiol-redox pathways in bacteria. Annu. Rev. Microbiol. *55*, 21–48.

Saini, V., Cumming, B.M., Guidry, L., Lamprecht, D.A., Adamson, J.H., Reddy, V.P., Chinta, K.C., Mazorodze, J.H., Glasgow, J.N., Richard-Greenblatt, M., et al. (2016). Ergothioneine maintains redox and bioenergetic homeostasis essential for drug susceptibility and virulence of *Mycobacterium tuberculosis*. Cell Rep. *14*, 572–585.

Sakrak, O., Kerem, M., Bedirli, A., Pasaoglu, H., Akyurek, N., Ofluoglu, E., and Gültekin, F.A. (2008). Ergothioneine modulates proinflammatory cytokines and heat shock Protein 70 in mesenteric ischemia and reperfusion injury. J. Surg. Res. *144*, 36–42.

Salama, N.R., Hartung, M.L., and Müller, A. (2013). Life in the human stomach: persistence strategies of the bacterial pathogen *Helicobacter pylori*. Nat. Rev. Microbiol. *11*, 385–399.

Salama, N.R., Otto, G., Tompkins, L., and Falkow, S. (2001). Vacuolating cytotoxin of *Helicobacter pylori* plays a role during colonization in a mouse model of infection. Infect. Immun. *69*, 730–736.

Schiefner, A., Breed, J., Bösser, L., Kneip, S., Gade, J., Holtmann, G., Diederichs, K., Welte, W., and Bremer, E. (2004a). Cation-pi interactions as determinants for binding of the compatible solutes glycine betaine and proline betaine by the periplasmic ligand-binding protein ProX from *Escherichia coli*. J. Biol. Chem. *279*, 5588–5596.

Schiefner, A., Holtmann, G., Diederichs, K., Welte, W., and Bremer, E. (2004b). Structural basis for the binding of compatible solutes by ProX from the hyperthermophilic archaeon *Archaeoglobus fulgidus*. J. Biol. Chem. *279*, 48270–48281.

Schofield, W.B., Zimmermann-Kogadeeva, M., Zimmermann, M., Barry, N.A., and Goodman, A.L. (2018). The stringent response determines the ability of a commensal bacterium to survive starvation and to persist in the gut. Cell Host Microbe *24*, 120–132.e6.

Schuster, C.F., Bellows, L.E., Tosi, T., Campeotto, I., Corrigan, R.M., Freemont, P., and Gründling, A. (2016). The second messenger c–di-amp inhibits the osmolyte uptake system OpuC in *Staphylococcus aureus*. Sci. Signal. *9*, ra81.

Seebeck, F.P. (2010). *In vitro* reconstitution of mycobacterial ergothioneine biosynthesis. J. Am. Chem. Soc. *132*, 6632–6633.

Sies, H., and Jones, D.P. (2020). Reactive oxygen species (ROS) as pleiotropic physiological signalling agents. Nat. Rev. Mol. Cell Biol. *21*, 363–383.

Smith, E., Ottosson, F., Hellstrand, S., Ericson, U., Orho-Melander, M., Fernandez, C., and Melander, O. (2020). Ergothioneine is associated with reduced mortality and decreased risk of cardiovascular disease. Heart *106*, 691–697.

Tang, R.M.Y., Cheah, I.K.-M., Yew, T.S.K., and Halliwell, B. (2018). Distribution and accumulation of dietary ergothioneine and its metabolites in mouse tissues. Sci. Rep. *8*, 1601.

Taubert, D., Jung, N., Goeser, T., and Schömig, E. (2009). Increased ergothioneine tissue concentrations in carriers of the Crohn's disease risk-associated 503F variant of the organic cation transporter OCTN1. Gut *58*, 312–314.

Terry, K., Williams, S.M., Connolly, L., and Ottemann, K.M. (2005). Chemotaxis plays multiple roles during *Helicobacter pylori* animal infection. Infect. Immun. *73*, 803–811.

Teruya, T., Chen, Y.-J., Kondoh, H., Fukuji, Y., and Yanagida, M. (2021). Whole-blood metabolomics of dementia patients reveal classes of disease-linked metabolites. Proc. Natl. Acad. Sci. USA *118*, e2022857118.

Terwilliger, T.C. (1999). Reciprocal-space solvent flattening. Acta Crystallogr. D Biol. Crystallogr. *55*, 1863–1871.

Tokuhiro, S., Yamada, R., Chang, X., Suzuki, A., Kochi, Y., Sawada, T., Suzuki, M., Nagasaki, M., Ohtsuki, M., Ono, M., et al. (2003). An intronic SNP in a RUNX1 binding site of *SLC22A4*, encoding an organic cation transporter, is associated with rheumatoid arthritis. Nat. Genet. *35*, 341–348.

Uhlén, M., Fagerberg, L., Hallström, B.M., Lindskog, C., Oksvold, P., Mardinoglu, A., Sivertsson, Å., Kampf, C., Sjöstedt, E., Asplund, A., et al. (2015). Proteomics. Tissue-based map of the human proteome. Science *347*, 1260419.

Ulfig, A., and Leichert, L.I. (2021). The effects of neutrophil-generated hypochlorous acid and other hypohalous acids on host and pathogens. Cell. Mol. Life Sci. *78*, 385–414.

Ulrich, K., and Jakob, U. (2019). The role of thiols in antioxidant systems. Free Radic. Biol. Med. *140*, 14–27.

Van Laer, K., Hamilton, C.J., and Messens, J. (2013). Low-molecular-weight thiols in thiol-disulfide exchange. Antioxid. Redox Signal. *18*, 1642–1653.

Vaneechoutte, M., Kämpfer, P., De Baere, T., Avesani, V., Janssens, M., and Wauters, G. (2007). *Chryseobacterium hominis* sp. nov., to accommodate clinical isolates biochemically similar to CDC groups II-h and II-c. Int. J. Syst. Evol. Microbiol. *57*, 2623–2628.

Velasquez, M.T., Ramezani, A., Manal, A., and Raj, D.S. (2016). Trimethylamine *N*-oxide: the good, the bad and the unknown. Toxins *8*, 326.

Volk, C. (2014). OCTs, OATs, and OCTNs: structure and function of the polyspecific organic ion transporters of the SLC22 family. Wiley Interdiscip. Rev. Membr. Transp. Signal. *3*, 1–13.

Walsh, B.J.C., and Giedroc, D.P. (2020). H_2S and reactive sulfur signaling at the host-bacterial pathogen interface. J. Biol. Chem. *295*, 13150–13168.

Wang, G., Alamuri, P., and Maier, R.J. (2006). The diverse antioxidant systems of *Helicobacter pylori*. Mol. Microbiol. *61*, 847–860.

Weiss, M.S. (2001). Global indicators of X-ray data quality. J. Appl. Crystallogr. *34*, 130–135.

Weiss, S.J. (1989). Tissue destruction by neutrophils. N. Engl. J. Med. *320*, 365–376.

Wilkens, S. (2015). Structure and mechanism of ABC transporters. F1000Prime Rep. *7*, 14.

Williamson, R.D., McCarthy, F.P., Manna, S., Groarke, E., Kell, D.B., Kenny, L.C., and McCarthy, C.M. (2020). L-(+)-Ergothioneine significantly improves the clinical characteristics of preeclampsia in the reduced uterine perfusion pressure rat model. Hypertension *75*, 561–568.

Winter, S.E., Thiennimitr, P., Winter, M.G., Butler, B.P., Huseby, D.L., Crawford, R.W., Russell, J.M., Bevins, C.L., Adams, L.G., Tsolis, R.M., et al. (2010). Gut inflammation provides a respiratory electron acceptor for *Salmonella*. Nature *467*, 426–429.

Wollert, T., Pasche, B., Rochon, M., Deppenmeier, S., van den Heuvel, J., Gruber, A.D., Heinz, D.W., Lengeling, A., and Schubert, W.D. (2007). Extending the host range of *Listeria monocytogenes* by rational protein design. Cell *129*, 891–902.

Wu, L.-Y., Cheah, I.K., Chong, J.R., Chai, Y.L., Tan, J.Y., Hilal, S., Vrooman, H., Chen, C.P., Halliwell, B., and Lai, M.K.P. (2021). Low plasma ergothioneine levels are associated with neurodegeneration and cerebrovascular disease in dementia. Free Radic. Biol. Med. *177*, 201–211.

Yang, D.C., Blair, K.M., Taylor, J.A., Petersen, T.W., Sessler, T., Tull, C.M., Leverich, C.K., Collar, A.L., Wyckoff, T.J., Biboy, J., et al. (2019). A genome-wide *Helicobacter pylori* morphology screen uncovers a membrane-spanning helical cell shape domplex. J. Bacteriol. *201*, e00724–e00718.

Zhou, W., Whiteley, A.T., de Oliveira Mann, C.C., Morehouse, B.R., Nowak, R.P., Fischer, E.S., Gray, N.S., Mekalanos, J.J., and Kranzusch, P.J. (2018). Structure of the human cGAS–DNA complex reveals enhanced control of immune surveillance. Cell *174*, 300–311.e11.

Zimmermann, M., Zimmermann-Kogadeeva, M., Wegmann, R., and Goodman, A.L. (2019). Mapping human microbiome drug metabolism by gut bacteria and their genes. Nature *570*, 462–467.

Please cite this article in press as: Dumitrescu et al., A microbial transporter of the dietary antioxidant ergothioneine, Cell (2022), https://doi.org/10.1016/j.cell.2022.10.008

STAR★METHODS

KEY RESOURCES TABLE

REAGENT or RESOURCE	SOURCE	IDENTIFIER
Bacterial and virus strains		
Table S4	This paper	N/A
Biological samples		
Human fecal samples	Gift from Andrew Goodman (Yale University School of Medicine), (Zimmermann et al., 2019)	N/A
Chemicals, peptides, and recombinant proteins		
(L)-(+)-Ergothioneine (EGT)	Sigma-Aldrich	Cat# E7521
(L)-(+)-Ergothioneine (EGT)	Cayman Chemical	Item# 14905
(L)-(+)-Ergothioneine-d^3 (EGT-d^3)	Toronto Research Chemicals	Cat# E600002
(L)-(+)-Ergothioneine-d^9 (EGT-d^9)	Toronto Research Chemicals	Cat# E600003
Trimethylamine-d^9 hydrochloride (TMA-d^9)	Toronto Research Chemicals	Cat# T795807
Bromobimane (mBBr)	Sigma-Aldrich	Cat# B4380
Bromobimane (mBBr)	Santa Cruz Biotechnology	Cat# sc-214629A
Diethylenetriaminepentaacetic acid (DTPA)	Sigma-Aldrich	Cat# D6518
Tris(2-carboxyethyl)phosphine hydrochloride (TCEP)	Sigma-Aldrich	Cat# C4706
L-Cysteine	Sigma-Aldrich	Cat# 168149
L-Histidine	Sigma-Aldrich	Cat# H8000
L-Methionine	Sigma-Aldrich	Cat# M9625
L-Proline	Sigma-Aldrich	Cat# P5607
Betaine (Glycine betaine)	Sigma-Aldrich	Cat# B2629
Choline chloride	Sigma-Aldrich	Cat# C7527
L-Carnitine	Sigma-Aldrich	Cat# C0283
2-mercaptoethanol (BME)	Sigma-Aldrich	Cat# M6250
Acetonitrile (ACN)	Sigma-Aldrich	Cat# 34851
Pierce 0.1% Formic acid (v/v) in Acetonitrile, LC-MS grade	Thermo Fisher	Cat# 85174
Pierce 0.1% Formic acid (v/v) in Water, LC-MS grade	Thermo Fisher	Cat# 85170
Imidazole	Fisher Scientific	Cat# AC122025000
L-Arabinose	Sigma	Cat# A3256
Methanol, LC-MS grade	VWR	Cat# JT9830-2
S-adenosylmethionine (SAM)	New England Biolabs	Cat# B9003S
L-Methionine (*methyl*-^{13}C)	Cambridge Isotope Laboratories	Item# CLM-206-PK
Isopropyl β-D-1-thiogalactopyranoside (IPTG)	AmericanBio	Cat# AB00841-00010
Brucella broth	Fisher Scientific	Cat# B11088
Gibco heat-inactivated fetal bovine serum (HI-FBS)	Fisher Scientific	Cat# 16140071
Columbia blood agar base	Fisher Scientific	Cat# OXCM331B
LB agar, miller	Fisher Scientific	Cat# DF045-17-4
LB broth, miller	Fisher Scientific	Cat# BP1426-500
Defibrinated horse blood	VWR	Cat# 10052-754
Vancomycin hydrochloride	Sigma-Aldrich	Cat# V2002
Cefsulodin sodium salt hydrate	Sigma-Aldrich	Cat# C8145
Polymyxin B sulfate salt	Sigma-Aldrich	Cat# P1004
Cycloheximide	Sigma-Aldrich	Cat# C7698

(*Continued on next page*)

Please cite this article in press as: Dumitrescu et al., A microbial transporter of the dietary antioxidant ergothioneine, Cell (2022), https://doi.org/10.1016/j.cell.2022.10.008

Continued

REAGENT or RESOURCE	SOURCE	IDENTIFIER
Trimethoprim	Sigma-Aldrich	Cat# T7883
Amphotericin B	Fisher Scientific	Cat# BP928-250
β-cyclodextrin	Sigma-Aldrich	Cat# C4805
Chloramphenicol	Sigma-Aldrich	Cat# C0378
Kanamycin	Fisher Scientific	Cat# AAJ67354AE
Metronidazole	Sigma-Aldrich	Cat# M3761
Nalidixic acid	Sigma-Aldrich	Cat# N8878
Bacitracin	Sigma-Aldrich	Cat# B0125
Streptomycin sulfate	Fisher Scientific	Cat# AAJ6129922
Difco brain heart infusion (BHI)	Fisher Scientific	Cat# 10462498
Gentamicin sulfate salt	Sigma-Aldrich	Cat# G1264
HEPES	AmericanBio	Cat# AB00892-01000
10x phosphate buffered saline (PBS)	Fisher Scientific	Cat# BP3994
EDTA-free protease inhibitor cocktail	Sigma-Aldrich	Cat# 11836170001
Benzonase	Sigma-Aldrich	Cat# E8263
Sodium hypochlorite solution	Sigma-Aldrich	Cat# 425044
Hydrogen peroxide solution	Sigma-Aldrich	Cat# 88597
Gibco DMEM	ThermoFisher Scientific	Cat# 11995065
His_6-$EgtU^{SBD}$	This paper	N/A
His_6-$EgtU^{SBD}$ Y390F	This paper	N/A
His_6-$EgtU^{SBD}$ Y390A	This paper	N/A
His_6-$EgtU^{SBD}$ R454E	This paper	N/A
His_6-$EgtU^{SBD}$ R454A	This paper	N/A
Critical commercial assays		
Q5 Site-Directed Mutagenesis Kit	New England Biolabs	Cat# E0552S
Deposited data		
Primary sequence of *H. pylori* EgtU	Baltrus et al., 2009	GenBank: ACI27532.1
Primary sequence of *H. pylori* EgtV	Baltrus et al., 2009	GenBank: ACI27533.1
Primary sequence of *E. coli* ProX	GenBank	GenBank: ECK2673
Primary sequence of *C. difficile* CD630_32160	GenBank	GenBank: CAJ70113.1
Primary sequence of *S. enterica* OsmX	Jarvik et al., 2010	GenBank: ACY88277.1
Primary sequence of *S. enterica* YehZ	Jarvik et al., 2010	GenBank: ACY89112.1
Crystal structure of *H. pylori* EgtU SBD	This paper	PDB: 8DP6
Crystal structure of *H. pylori* EgtU SBD–EGT	This paper	PDB: 8DP7
Crystal structure of *E. coli* ProX–glycine betaine	Schiefner et al., 2004a	PDB: 1R9L
Experimental models: Cell lines		
Human gastric epithelial AGS cells	ATCC	CRL-1739
Experimental models: Organisms/strains		
Mouse: C57BL/6J	Jackson Laboratories	Strain# 000664
Oligonucleotides		
Table S5	This paper	N/A
Recombinant DNA		
Table S6	This paper	N/A
Software and algorithms		
MassHunter Quantitative Analysis Software Version B.07.00	Agilent	N/A
MassHunter Optimizer	Agilent	N/A

(*Continued on next page*)

Continued

REAGENT or RESOURCE	SOURCE	IDENTIFIER
Origin 7.0	OriginLab	N/A
Phenix 1.19.2	Adams et al., 2010	https://phenix-online.org/
Coot 0.8.9.2	Emsley and Cowtan, 2004	https://www2.mrc-lmb.cam.ac.uk/personal/pemsley/coot/
PyMol v2.5.2	Schrodinger	https://pymol.org/2/
Geneious Prime 8	Geneious	N/A
Adobe Illustrator 2020	Adobe Creative Cloud	N/A
ChemDraw 20.0	PerkinElmer	N/A
Prism 9.1.2	GraphPad	N/A
Promals3D	Pei et al., 2008	http://prodata.swmed.edu/promals3d/promals3d.php
Other		
Oxoid CampyGen 2.5L Sachet	Fisher Scientific	Cat# OXCN0025A
BD GasPak 100 Systems	Fisher Scientific	Cat# 11-814-21
Anaerobic chamber	Coy Laboratory Products	N/A
6550 iFunnel quadrupole time-of-flight (qTOF) mass spectrometer	Agilent	N/A
C18 (100 Å) 5 μm (250 x 4.6 mm) column	Phenomenex	Part# 00G-4601-E0
6490 triple quadrupole mass spectrometer	Agilent	N/A
C18 UPLC (100 Å) 1.7 μm (100 x 2.1 mm) column	Phenomenex	Part# 00D-4475-AN
HILIC UPLC column (100 Å) 1.7 μm (100 x 2.1 mm)	Phenomenex	Part# 00D-4474-AN
LM20 Microfluidizer	Microfluidics	N/A
French Pressure Cell Press	Thermo Fisher	N/A
ÄKTA pure chromatography system	GE Healthcare	N/A
HisTrap FF column	Fisher Scientific	Cat# 45-000-336
Superdex 200 10/300 GL (gel filtration column)	Cytiva	Cat# 2890944
VP-ITC calorimeter	Microcal	N/A

RESOURCE AVAILABILITY

Lead contact

Further information and requests for resources and reagents should be directed to and will be fulfilled by the lead contact, Stavroula Hatzios (stavroula.hatzios@yale.edu).

Materials availability

All unique/stable reagents generated in this study are available from the lead contact with a completed Materials Transfer Agreement.

Data and code availability

- *Apo* and ligand-bound crystal structures of the EgtU SBD have been deposited in the Protein Data Bank. Accession numbers are listed in the key resources table. Raw mass spectrometry data files are available from the lead contact upon request.
- This paper does not report original code.
- Any additional information required to reanalyze the data reported in this paper is available from the lead contact upon request.

EXPERIMENTAL MODEL AND SUBJECT DETAILS

Bacterial strains and growth conditions

Bacterial strains, plasmids, and primers used in this study are summarized in Tables S4–S6. *H. pylori* strains were grown as previously described (Salama et al., 2001). Briefly, *H. pylori* was cultured at 37 °C under microaerophilic conditions using a 2.5 L gas pack jar containing a CampyGen sachet or a humidified incubator set to 10% CO_2. Broth cultures were prepared using Brucella broth supplemented with 10% (v/v) heat-inactivated fetal bovine serum (HI-FBS; Gibco, Catalog no. 16140071). *H. pylori* was also cultured on Columbia blood agar (Oxoid) plates supplemented with 5% (v/v) horse blood (VWR) and 10 μg/mL vancomycin hydrochloride,

5 μg/mL cefsulodin sodium hydrate, 0.33 μg/mL polymyxin B sulfate, 50 μg/mL cycloheximide, 10 μg/mL trimethoprim, 16 μg/mL amphotericin B, and 2 μg/mL β-cyclodextrin. Plates were further supplemented with 25 μg/mL chloramphenicol, 50 μg/mL kanamycin, 36 μg/mL metronidazole, 90 μg/mL vancomycin hydrochloride, 10 μg/mL nalidixic acid, and/or 100 μg/mL bacitracin as needed. *Campylobacter jejuni* was grown under the same conditions as *H. pylori*. *Bacteroides thetaiotaomicron* was grown in TYG liquid media or on Brain Heart Infusion (BHI) agar plates supplemented with 5% (v/v) horse blood and 200 μg/mL gentamicin sulfate salt in a Coy anaerobic chamber (20% CO_2, 10% H_2, and 70% N_2) as previously described (Schofield et al., 2018). *L. monocytogenes* was grown on BHI agar plates supplemented with 200 μg/mL streptomycin sulfate or in BHI liquid medium. *S. enterica*, *Vibrio cholerae*, and *E. coli* were grown at 37 °C in LB medium or on LB agar plates supplemented with 20 μg/mL chloramphenicol or 50 μg/mL kanamycin, carbenicillin, or ampicillin as needed. *C. difficile* was grown on BHI agar plates supplemented with 0.5% (w/v) yeast extract and 0.1% (w/v) L-cysteine (BHIS) with taurocholate (0.1% (w/v); 1.9 mM), thiamphenicol (10–15 μg/mL), kanamycin (50 μg/mL), or cefoxitin (8 μg/mL) as needed. *C. difficile* defined medium (CDDM) (Karasawa et al., 1995) was supplemented with 5-fluoroorotic acid at 2 mg/mL and uracil at 5 μg/mL. Cultures were grown at 37 °C under anaerobic conditions using a gas mixture containing 85% N_2, 5% CO_2 and 10% H_2.

Overnight cultures were prepared by inoculating the appropriate liquid medium with cells from dense patches of bacteria expanded from a single colony (*H. pylori*, *C. jejuni*) or with a single colony (*E. coli*, *S. enterica*, *V. cholerae*, *B. thetaiotaomicron*, *L. monocytogenes*). Cultures were grown for 16–18 h at 37 °C with shaking at 100 r.p.m. (*H. pylori*, *C. jejuni*), 250 r.p.m. (*E. coli*, *S. enterica*, *V. cholerae*, *L. monocytogenes*), or as static cultures (*B. thetaiotaomicron*). Starter cultures of *C. difficile* were prepared by inoculating BHIS broth with a single colony, followed by static incubation at 37 °C for 3 h under anaerobic conditions. Unless otherwise specified, cultures were subsequently diluted into fresh medium as follows: *H. pylori* and *C. jejuni* cultures were diluted to a starting OD_{600} of 0.1; *E. coli*, *S. enterica*, *L. monocytogenes* and *V. cholerae* were diluted 1:1000; *B. thetaiotaomicron* was diluted 1:100; *C. difficile* was diluted 1:50. For assays testing for EGT biosynthesis, *H. pylori* cultures were supplemented with 1 mM His or Met, or with 0.2 mM Cys, as higher concentrations of Cys inhibited *H. pylori* growth. For assays testing for biosynthetic incorporation of ^{13}C-Met into EGT, *H. pylori* cultures were supplemented with 10 mM Met or ^{13}C-Met. For EGT-d^3 transport assays, *H. pylori* cultures were supplemented with 0, 1, or 5 μg of EGT-d^3, whereas *E. coli*, *S. enterica*, *V. cholerae*, *C. jejuni*, *B. thetaiotaomicron*, *L. monocytogenes*, and *C. difficile* cultures were supplemented with 0.2 μg/mL of EGT-d^3. Cultures of *E. coli* and *S. enterica* strains containing pBAD vectors were supplemented with 0.2% (w/v) L-arabinose to induce protein expression. To estimate EGT concentrations in *H. pylori*, cells were approximated as cylinders ($V = \pi r^2 l$) with $l = 3.5$ μm and $r = 0.5$ μm.

Mammalian cell lines and growth conditions

Human gastric epithelial AGS cells (ATCC CRL-1739; derived from a female patient) were cultured in Dulbecco's Modified Eagle's Medium (DMEM; Gibco) supplemented with 10% (v/v) HI-FBS at 37 °C in a humidified 5% CO_2 incubator.

Mouse experiments

All animal protocols were reviewed and approved by the Yale University Institutional Animal Care and Use Committee. Female 6-week-old C57BL/6J mice were purchased from Jackson Laboratories (Bar Harbor, ME). Mice were group housed and randomly assigned to experimental groups. Animals were monitored daily by veterinary staff from the Yale Animal Resources Center.

Human fecal samples

Human fecal samples from 25 healthy individuals were collected under Yale University Human Investigation Committee protocol number 1106008725 at the Yale University School of Medicine. Information regarding age, gender, eligibility criteria, and collection/storage methods were reported previously (Goodman et al., 2011; Zimmermann et al., 2019).

METHOD DETAILS

Strain and plasmid construction

H. pylori mutant strains were generated by natural transformation with a linear PCR construct or genomic DNA (gDNA) containing the flanking regions of the targeted gene and a kanamycin or chloramphenicol resistance cassette as previously described (Salama et al., 2001). Complemented strains were generated by naturally transforming the relevant mutant strain with a linear PCR product or plasmid containing the full coding region of the relevant gene followed by a kanamycin or chloramphenicol resistance cassette. The transformed construct replaced the antibiotic resistance cassette at the native locus of the gene. To complement mutant strains at a nonnative site, genes were cloned into vector pLC292, which contains the coding region of the *H. pylori rdxA* gene with an internal multiple cloning site (Terry et al., 2005). The plasmid was then transformed into the appropriate *H. pylori* mutant, and the complemented strain was selected via metronidazole resistance, which results from genetic recombination into the endogenous *rdxA* locus. All *H. pylori* mutant and complemented strains were verified by locus-specific PCR reactions and DNA sequencing.

H. pylori G27MA *HPG27_777::Tn* and Δ*HPG27_885* were generated by transforming *H. pylori* G27MA with gDNA from the corresponding *H. pylori* G27 mutant strain. *H. pylori* G27 mutant strains were obtained from a previously generated mutant library containing transposon insertion mutants marked with a chloramphenicol acetyl transferase (*cat*) cassette (e.g., *HPG27_777::Tn*) and targeted deletion mutants marked with the *cat* cassette (e.g., Δ*HPG27_885*) (Yang et al., 2019).

To construct *H. pylori* G27MA Δ*egtU*, the 500-bp DNA sequences flanking *HPG27_777* (GenBank ACI27532.1) were amplified from *H. pylori* G27MA gDNA using primers DD-75 and DD-76 (upstream flank) and DD-78 and DD-105 (downstream flank). The *Campylobacter coli cat* cassette was amplified from *H. pylori* G27MA Δ*cagA* gDNA (gift of Manuel Amieva, Stanford University School of Medicine) using primers DD-73 and DD-104. A consensus *H. pylori* ribosome binding site (TCTAAGGAGAAT) was added to the 3' end of the *cat* cassette to maintain translation of the downstream *HPG27_778* gene. The resulting PCR products were gel-purified and assembled into a single linear construct via splicing by overlap extension PCR using primers DD-75 and DD-78, and the product was transformed into WT *H. pylori* G27MA.

To construct *H. pylori* G27MA Δ*egtV*, the 500-bp DNA sequences flanking *HPG27_778* (GenBank ACI27533.1) were amplified from *H. pylori* G27MA gDNA using primers DD-79 and DD-80 (upstream flank) and DD-81 and DD-82 (downstream flank). The *C. coli cat* cassette was amplified from *H. pylori* G27MA Δ*cagA* gDNA using primers DD-73 and DD-74. The resulting PCR products were gel-purified and assembled into a single linear construct via splicing by overlap extension PCR using primers DD-79 and DD-82, and the product was transformed into WT *H. pylori* G27MA.

The *H. pylori* Δ*egtU::egtU* complemented strain was generated via transformation of plasmid pUC57_*egtU::egtU-kan* into *H. pylori* G27MA Δ*egtU*. Plasmid pUC57_*egtU::egtU-kan* was custom synthesized by GenScript and contains a 4,075-bp insert comprised of the 500-bp sequence upstream of *HPG27_777* followed by the complete *HPG27_777* coding region, a kanamycin resistance cassette, and the first 497 bp of the *HPG27_778* coding region.

The *H. pylori* Δ*egtV rdxA::egtV* complemented strain was generated via transformation of plasmid pLC292_*egtV* into *H. pylori* G27MA Δ*egtV*. To construct pLC292_*egtV*, *HPG27_778* was PCR amplified from *H. pylori* G27MA gDNA using primers DD-152 and DD-153. The PCR product was cloned into XbaI/PstI-digested pLC292 (Terry et al., 2005) using Gibson assembly (Gibson et al., 2009). pLC292_*egtV* was electroporated into *E. coli* DH5α*λpir* and the resulting plasmid was sequence verified prior to transformation into *H. pylori* G27MA Δ*egtV*.

To construct the *H. pylori* Δ*egtV::egtV* complemented strain, a 1200-bp DNA sequence including the 500-bp sequence upstream of *HPG27_778* and the complete *HPG27_778* coding region was amplified using primers DD-79 and DD-91. The 500-bp sequence downstream of *HPG27_778* was amplified using primers DD-145 and DD-82. A kanamycin resistance cassette was amplified from *H. pylori* G27MA Δ*vacA* (gift of Manuel Amieva, Stanford University School of Medicine) using primers DD-84 and DD-85. The PCR products were purified and assembled into a single transformation product via splicing by overlap extension PCR using primers DD-79 and DD-82, and the resulting product was transformed into *H. pylori* G27MA Δ*egtV*.

To construct *H. pylori* PMSS1 Δ*egtV*, the ~1.8-kb linear construct used to generate *H. pylori* G27MA Δ*egtV* was amplified from *H. pylori* G27MA Δ*egtV* gDNA using primers DD-79 and DD-82. The PCR product was treated with cell-free PMSS1 lysates as previously described (Donahue et al., 2000; Fung et al., 2019) and then transformed into PMSS1. To construct the *H. pylori* PMSS1 Δ*egtV::egtV* complemented strain, the ~3.1-kb linear construct used to generate *H. pylori* G27MA Δ*egtV::egtV* was amplified from *H. pylori* G27MA Δ*778::778* gDNA using primers DD-79 and DD-82. The PCR product was treated with cell-free PMSS1 lysates and then transformed into *H. pylori* PMSS1 Δ*egtV*.

The WT *C. difficile* strain used was 630Δ*erm* and deletion mutants of *CD630_32160* and *opuCC* were constructed using *C. difficile* 630Δ*erm*Δ*pyrE* as the parental strain via *pyrE*-based allele-coupled exchange (Ng et al., 2013), using uracil and 5-fluoroorotic acid to select for plasmid excision as previously described (Donnelly et al., 2017). Complementation strains were constructed as previously described (Donnelly et al., 2017) using CDDM to select for restoration of *pyrE* resulting from insertion of the plasmid carrying the complementation construct and *pyrE*. The Δ*CD630_32160*Δ*opuCC* strain was constructed by first deleting *CD630_32160*, then *opuCC*.

To construct pMTL-YN3-Δ*CD630_32160*, primers EF-3448 and EF-3445 were used to amplify 669 bp upstream of *CD630_32160* through the first 39 bp of *CD630_32160*. Primers EF-3444 and EF-3449 were used to amplify the last 249 bp of *CD630_32160* through the 378 bp downstream of *CD630_32160*. These fragments were cloned into AscI/SbfI-digested pMTL-YN3 using Gibson assembly. The product was transformed into *E. coli* DH5α and sequence verified. The resulting plasmid was transformed into HB101/pRK24 for conjugation with *C. difficile*.

To construct pMTL-YN3-Δ*opuCC*, primers EF-3441 and EF-3436 were used to amplify 636 bp upstream of *opuCC* through the first 90 bp of *opuCC*. Primers EF-3435 and EF-3442 were used to amplify the last 48 bp of *opuCC* through the 662 bp downstream of *opuCC*. These fragments were cloned into AscI/SbfI-digested pMTL-YN3 using Gibson assembly. The product was transformed into *E. coli* DH5α and sequence verified. The resulting plasmid was transformed into HB101/pRK24 for conjugation with *C. difficile*.

To construct pMTL-YN1C-P_{opuCC}*::opuCC*, primers EF-3900 and EF-3901 were used to amplify 200 bp upstream of *opuCC* as a promoter. Primers EF-3902 and EF-3903 were used to amplify *opuCC*. These fragments were cloned into NotI/ZhoI-digested pMTL-YN1C using Gibson assembly. The product was transformed into *E. coli* DH5α and sequence verified. The resulting plasmid was transformed into HB101/pRK24 for conjugation with *C. difficile*.

To construct pMTL-YN1C-P_{CD630_32160}*::CD630_32160*, primers EF-3904 and EF-3905 were used to amplify 200 bp upstream of *CD630_32160* as a promoter through *CD630_32160*. This fragment was cloned into NotI/ZhoI-digested pMTL-YN1C using Gibson assembly. The product was transformed into *E. coli* DH5α and sequence verified. The resulting plasmid was transformed into HB101/pRK24 for conjugation with *C. difficile*.

To construct *E. coli* Δ*yehZ* + pBAD.*yehZEc* and *S. enterica* Δ*yehZ* + pBAD.*yehZSe*, the *yehZ* gene (*E. coli*, Genbank ECK2124; *S. enterica*, Genbank ACY89112.1) was cloned from *E. coli* and *S. enterica* gDNA using primers DD-206 and DD-207 or DD-208

and DD-209, respectively. The resulting PCR products were cloned by Gibson assembly into pBAD33 digested with Eco53kI. The resulting constructs were then electroporated into *E. coli* Δ*yehZ* and *S. enterica* Δ*yehZ*.

To construct *E. coli* BL21 pET28b*His*$_6$-*egtU*^{SBD}, the gene sequence encoding the predicted solute-binding domain of HPG27_777 (nt 844-1662) was PCR amplified from *H. pylori* G27MA gDNA using primers DD-132 and DD-127. The resulting PCR product was reamplified using primers DD-126 and DD-127 to install an N-terminal His$_6$ tag, and then reamplified a second time using primers DD-128 and DD-133 to install sequences complementary to the pET28b vector for Gibson assembly. The final product was cloned by Gibson assembly into NcoI/NheI-digested pET28b. All sequenced clones encoded the following amino-acid substitutions compared to the deposited HPG27_777 sequence (GenBank 27532.1), likely reflecting genomic differences between *H. pylori* G27 and *H. pylori* G27MA: M334V, L412F, Q415P, and I503T. Plasmid pET28b*His*$_6$-*egtU*^{SBD} was then transformed into *E. coli* OneShot BL21(DE3)pLysS by heat shock. Amino-acid substitution mutants in the EgtU SBD were generated with the Q5® Site-Directed Mutagenesis Kit (NEB) according to manufacturer's instructions using pET28b.*His*$_6$-*egtU*^{SBD} as template and primers listed in Table S5. Constructs were transformed into *E. coli* OneShot BL21(DE3)pLysS by heat shock. Mutations encoding the desired amino-acid substitutions were confirmed by DNA sequencing.

To construct *E. coli* BL21 DE3 RL1 pET16-*egtU*^{SBD}, the gene sequence encoding the predicted SBD of HPG27_777 (nt 844-1662) was synthesized as a linear fragment (IDT) and cloned by Gibson assembly into a custom BamHI/NotI-digested pET16 vector (Zhou et al., 2018) that tags the inserted sequence with a His$_6$-SUMO2 fusion tag. The product was transformed into *E. coli* BL21 DE3 RL1 and confirmed by DNA sequencing.

Metabolite extraction and thiol labeling

Starter cultures were diluted into fresh medium as specified above, then grown for an additional 4–6 h under the same conditions. Cultures of the same species within a given experiment were subsequently normalized by OD_{600} and centrifuged (3200 x *g*, 4 °C, 10 min). A portion of each culture was collected prior to harvesting for the enumeration of colony-forming units (CFU). Cell pellets were washed twice with phosphate-buffered saline (PBS) and then resuspended in 500 μL extraction buffer (cold 50 mM HEPES, 50% ACN (v/v), 1 mM DTPA, 1 mM TCEP, pH 8). For the analysis of culture supernatants or media-only controls, samples were centrifuged, and 1 mL of the supernatant was frozen at –80 °C and lyophilized. The lyophilized powder was then reconstituted in 500 μL extraction buffer and diluted 1:1 with sterile deionized and distilled water from an ELGA water purification system (ddH_2O). For mass spectrometry-based quantification of EGT or EGT-d^3, samples were supplemented with 1 μg of EGT-d^9, incubated at –20 °C for at least 30 min and then centrifuged (3200 x *g*, 4 °C, 10 min). The resulting supernatants were treated with 35 μL of 74 mM mBBr prepared in ACN and incubated in the dark for 15 min at 60 °C. Samples were then frozen, lyophilized, and stored at –80 °C until LC–MS analysis.

Liquid chromatography–mass spectrometry

Lyophilized samples were reconstituted in 500 μL methanol and cleared by centrifugation (10 min, 21,000 x *g*, room temperature) prior to LC–MS analysis. For untargeted metabolomics, high-resolution mass spectra were obtained on an Agilent 6550 iFunnel quadrupole time-of-flight (qTOF) mass spectrometer equipped with a 1290 dual spray electrospray ionization (ESI) source coupled to an Agilent 1290 high-performance liquid chromatography (HPLC) system. Samples (10 μL) were separated using a Phenomenex C18 (100 Å) 5 μm (250 x 4.6 mm) column under the following conditions: flow rate, 0.7 mL min^{-1}; mobile phase, H_2O/ACN gradient containing 0.1% (v/v) formic acid: 30 min 5–100% (v/v) ACN, 5 min at 100% (v/v) ACN, 0.1 min 100–5% (v/v) ACN, 2 min at 5% (v/v) ACN, 5 min post-time at 5% (v/v) ACN. The qTOF instrument was operated in positive scanning mode (20 – 1700 *m/z*) using the following source parameters: capillary voltage, 3500 V; nozzle voltage, 2000 V; gas temperature, 225 °C; gas flow, 12 L min^{-1}; nebulizer, 35 psi; sheath gas temperature, 275 °C; sheath gas flow, 12 L min^{-1}. Mass calibration was performed using a second ionization source and constant flow (5 μL min^{-1}) of reference solution (121.0509 *m/z* and 922.0098 *m/z*). Tandem MS/MS analysis of bimane-labeled EGT (mB-EGT) was performed using the same HPLC conditions and qTOF source parameters as described above. Targeted MS/MS of *m/z* = 420.1700 was performed using a mass tolerance of 10 ppm and a collision energy of 20, 30, 40, or 50 eV. All data were analyzed using Agilent MassHunter Quantitative Analysis Software Version B.07.00.

EGT levels were quantified by ESI triple quadrupole mass spectrometry (ESI-QQQ-MS). An Agilent 6490 Triple Quadrupole mass spectrometer was operating using positive ion electrospray ionization and Multiple Reaction Monitoring (MRM) to quantify specific target ions. Samples (5 μL) were separated using a Phenomenex C18 UPLC (100 Å) 1.7 μm (100 x 2.1 mm) column under the following conditions: flow rate, 0.3 mL min^{-1}; mobile phase, H_2O/ACN gradient containing 0.1% (v/v) formic acid: 15 min 5–20% (v/v) ACN, 1 min 20–100% (v/v) ACN, 5 min at 100% (v/v) ACN, 1 min 100–5% (v/v) ACN, 5 min post-time at 5% (v/v) ACN. The ESI-QQQ-MS was operated under the following source parameters: capillary voltage, 3500 V; nozzle voltage, 2000 V; gas temperature, 200 °C; gas flow, 12 L min^{-1}; sheath gas temperature, 200 °C; sheath gas flow, 12 L min^{-1}. Collision energies for fragmentation of mB-EGT were determined using the Agilent Mass Hunter Optimizer program. Precursor (*m/z*) to product ion (*m/z*) transitions and collision energies (eV) for each compound were as follows: mB-EGT: 420.17 → 185.1, 29 eV; mB-EGT-d^3: 423.19 → 188.1, 29 eV; mB-EGT-d^9: 429.23 → 194.1, 29 eV. Agilent MassHunter Quantitative Analysis Software Version B.07.00 was used for peak integration of fragment ions based on retention time and masses of chemical standards. EGT was quantified by comparing the area under the curve (AUC) values of light and heavy mB-EGT fragment ions. These values were then normalized by CFU where appropriate.

Please cite this article in press as: Dumitrescu et al., A microbial transporter of the dietary antioxidant ergothioneine, Cell (2022), https://doi.org/10.1016/j.cell.2022.10.008

TMA-d^9 levels were quantified by ESI-QQQ-MS using the same source parameters as used for the measurement of EGT. Samples (5 μL) were separated using a Phenomenex HILIC UPLC column (100 Å) 1.7 μm (100 x 2.1 mm) under the following conditions: flow rate, 0.3 mL min^{-1}; mobile phase, H_2O/ACN gradient containing 0.1% (v/v) formic acid: 2 min 95% (v/v) ACN, 4 min 95–50% (v/v) ACN, 3 min at 50% (v/v) ACN, 3 min 50–95% (v/v) ACN, 3 min at 95% (v/v) ACN, 5 min post-time at 95% (v/v) ACN. Collision energies for the fragmentation of TMA-d^9 were determined using Agilent Mass Hunter Optimizer program. Precursor (*m/z*) to product ion (*m/z*) transitions and collision energies (eV) used were TMA-d^9: 69.1 → 51.1, 26 eV. Agilent MassHunter Quantitative Analysis Software Version B.07.00 was used for peak integration of fragment ions based on retention time and masses of chemical standards. TMA-d^9 was quantified using a calibration curve of TMA-d^9 standard.

EgtU SBD purification for ITC analysis

Single colonies of *E. coli* OneShot BL21(DE3)pLysS containing pET28b*His$_6$-egtU^{SBD}* were used to inoculate 30-mL overnight cultures of LB medium containing 50 μg/mL kanamycin. Overnight cultures were diluted 1:100 in 1 L of LB medium containing 50 μg/mL kanamycin and grown at 37 °C with shaking at 250 r.p.m. to an OD_{600} of ~0.5–0.6. Expression was induced with 1 mM IPTG for 20 h at 15 °C with shaking at 200 r.p.m. Cells were harvested by centrifugation (20,000 x *g*, 4 °C, 30 min) and resuspended in ice-cold Buffer A (20 mM HEPES, 500 mM NaCl, 30 mM imidazole, 2 mM BME, pH 7.8; 3 mL/g of cells) supplemented with one complete EDTA-free protease inhibitor tablet (Sigma) and 3 μL benzonase (Sigma). Cells were lysed using an LM20 Microfluidizer (Microfluidics) operated at 15,000 psi or using a French Pressure Cell Press (Thermo) operated at 18,000 psi. The lysate was cleared by centrifugation (13,800 x *g*, 4 °C, 40 min), vacuum-filtered (0.22-μm filter), and loaded onto a 1-mL HisTrap FF column (GE Healthcare) equilibrated with Buffer A using an ÄKTA pure chromatography system (GE Healthcare). The sample was washed with 10 column volumes of Buffer A and eluted using a gradient of 0–100% 300 mM imidazole in Buffer A. Elution fractions (0.5 mL) were analyzed by SDS-PAGE and Coomassie staining. The relevant fractions were pooled and concentrated by centrifugation (3200 x *g*, 4 °C, 30 min) using Amicon Ultra-15 centrifugal filter units with an Ultracel-10 membrane (EMD Millipore). The concentrate was loaded onto a gel-filtration column equilibrated with Buffer B (20 mM HEPES, 150 mM NaCl, 2 mM BME, pH 7.8) using an ÄKTA pure chromatography system, and eluted with 1.5 column volumes of Buffer B. Elution fractions were analyzed by SDS-PAGE and Coomassie staining, and the fractions containing pure protein were pooled. Protein concentration was determined by UV absorbance at 280 nm using a calculated extinction coefficient of 27390 M^{-1} cm^{-1}.

ITC analysis

ITC was performed using a Microcal VP-ITC calorimeter under the following parameters: temperature, 30 °C; reference power, 10 μcal/s; spacing between injections, 360 s; injection volume, 2 μL first injection, 8 μL for the remaining injections, with a ligand concentration of 0.5 mM and a protein concentration of 20 μM. Protein solutions were dialyzed against Buffer B, and ligand solutions (EGT, glycine betaine, choline, proline, carnitine, and histidine) were prepared in the corresponding dialysate. Ligand and protein solutions were centrifuged (13,000 x *g*, 10 min, room temperature) and degassed prior to analysis. EGT–EgtU SBD titrations were performed in triplicate; titrations using EgtU SBD mutants, and control ligand titrations, were performed in duplicate. Data were background-subtracted using ligand-buffer reference titrations and fitted to a one set of sites model using Origin 7.0.

EgtU SBD purification for crystallography

Large (~1 L) M9ZB (0.5% glycerol, 1% Cas-amino Acids, 47.8 mM Na_2HPO_4, 22 mM KH_2PO_4, 18.7 mM NH_4Cl, 85.6 mM NaCl, 2mM $MgSO_4$, 100 mg/mL ampicillin, 34 mg/mL chloramphenicol, and trace metals) cultures were inoculated with overnight MDG culture (0.5% glucose, 25mM Na_2HPO_4, 25 mM KH_2PO_4, 50mM NH_4Cl, 5 mM Na_2SO_4, 2 mM $MgSO_4$, 0.25% aspartic acid, 100 mg/mL ampicillin, 34 mg/mL chloramphenicol, and trace metals) of *E. coli* BL21 DE3 RIL pET16-*egtU^{SBD}*, then grown for ~6 h before induction with 0.5 M IPTG overnight at 16 °C. Bacteria were harvested by centrifugation, resuspended in lysis buffer (20 mM HEPES-KOH pH 7.5, 400 mM NaCl, 30 mM imidazole, 10% glycerol, 1 mM DTT) and lysed on ice using a probe sonicator. Protein was bound to Ni-NTA resin (QIAGEN), washed with lysis buffer, wash buffer (lysis buffer supplemented to 1 M NaCl), then lysis buffer, before eluting with elution buffer (lysis buffer supplemented to 300 mM imidazole). Protein was dialyzed overnight with hSENP2 to remove imidazole and allow cleavage of the SUMO2 tag. Protein and tag were separated by size exclusion chromatography with a 16/600 Superdex 75 column in 250 mM KCl, 20 mM HEPES-KOH pH 7.5, and 1 mM TCEP, concentrated to ~130 mg/mL, then flash frozen with LiN_2, and stored at −80°C.

Selenomethionine-substituted protein was expressed and purified under similar conditions, with the following changes: large-scale M9ZB cultures were replaced with 47.8 mM Na_2HPO_4, 22 mM KH_2PO_4, 18.7 mM NH_4Cl, 85.6 mM NaCl, 0.4% D-glucose, 2 mM $MgSO_4$, 1 μg/mL thiamine-HCl, 100 mg/mL ampicillin, 34 mg/mL chloramphenicol, and trace metals. Approximately 20 min before induction, amino acids were added to the culture (50 mg/L leucine, isoleucine, valine; 100 mg/L phenylalanine, lysine, threonine; 75 mg/L selenomethionine), then cultures were induced as described above. In all buffers, 1 mM DTT was replaced with 1 mM TCEP.

Crystallization and structure determination

The *H. pylori* EgtU SBD (R282 to L553) was crystallized using the hanging drop method at 18 °C. Selenomethionine-substituted protein was diluted to 18 mg/mL, 45 mM KCl, 20 mM HEPES-KOH pH 7.5, and 1 mM DTT, then mixed 1:1 with 0.2 M sodium phosphate and 15% PEG-3350. Crystals were grown for 7 days then harvested in 0.2 M sodium phosphate, 15% PEG-3350, and 15% glycerol.

Native EgtU SBD (R282 to L553) was diluted to 14 mg/mL, 45 mM KCl, 20 mM HEPES-KOH pH 7.5, and 1 mM DTT, and mixed with 0.3 M ammonium sulfate, 22% PEG-4000, and 0.2 M sodium acetate pH 4.8. Crystals were grown for 2 days, then harvested in 0.3 M ammonium sulfate, 22% PEG-4000, 0.2 M sodium acetate pH 4.8, and 20% ethylene glycol.

Native EgtU SBD (R282 to L553) was also diluted to 14 mg/mL, 45 mM KCl, 20 mM HEPES-KOH pH 7.5, 1 mM DTT, and 5 mM EGT. Protein solution was mixed 1:1 with 0.2 M ammonium sulfate, 0.1 M sodium acetate, and 22% PEG-4000. Crystals were grown for 7 days and harvested in 0.2 M ammonium sulfate, 0.1 M sodium acetate pH 4.8, 22% PEG-4000, 20% ethylene glycol, and 10 mM EGT.

X-ray diffraction data were collected as part of the Northeast Collaborative Access Team at the Advanced Photon Source beamline 24-ID-E using a Dectris Eiger 16M detector. Data were processed using XDS and AIMLESS (Kabsch, 2010) using SSRL autoxds (A. Gonzalez, Stanford SSRL). Phase information for *apo* EgtU was collected using selenomethionine-substituted crystals. PHENIX HySS (Adams et al., 2010) found 4 sites, and a map was made using SOLVE/RESOLVE (Terwilliger, 1999). The models were built using Coot (Emsley and Cowtan, 2004) and refined using PHENIX. Crystallographic statistics are described in Table S3 (Chen et al., 2010; Karplus and Diederichs, 2012; Weiss, 2001).

Circular dichroism (CD) spectroscopy

The overall secondary structure of purified EgtU SBD was analyzed by CD using an Applied Photophysics Chirascan V100 instrument. Purified protein was buffer-exchanged from HEPES into PBS using 3 kDa MWCO Pierce™ Protein Concentrators (Thermo Fisher) via centrifugation for 30-min intervals at 4 °C and 15,000 x *g*. Protein was either used directly, or if thawed from frozen, centrifuged at 4 °C for 20 min at 20,000 x *g* to pellet any precipitate. A sample of supernatant was taken and denatured in 7.5 M guanidine hydrochloride and absorbance at 280 nm was measured. The concentration was determined using Beer's law with an extinction coefficient of 27,390 M^{-1} cm^{-1}. The protein was diluted to 15 μM in 400 μL total volume of PBS and loaded into a 1-mm path length quartz cuvette (Starna Cells). CD spectroscopy absorbance measurements were conducted at 20 °C from 190 – 300 nm wavelengths with a 1-nm step and 2-sec averaging time, resulting in 80,000 independent 25-μsec measurements. Measurements were performed in duplicate for each mutant, and data were corrected using a PBS blank. The raw absorbance (millidegrees, θ) was converted to Mean Residue Ellipticity ([θ]MR) using the following equation: [θ]MR = (100 x θ) / ((C x N) x l), where C is the molar protein concentration, N is the number of amino acids, and l is the cell path length in centimeters (Greenfield, 2006).

Bleach and peroxide assays

Overnight cultures of *H. pylori* were grown for 16–18 h at 37 °C, diluted to OD_{600} 0.1 in fresh medium, and grown for an additional 6 h at 37 °C. Cells (200 μL) were then treated with 2, 4, 5, or 10 mM sodium hypochlorite or an equivalent volume of ddH_2O in triplicate and incubated in a 96-well plate at 37 °C in a 10% CO_2 incubator. After 15 min, CFU were enumerated. The concentration of sodium hypochlorite was determined prior to each use by UV absorption at 293 nm using ε = 350 M^{-1} cm^{-1}. For peroxide assays, subcultures (5 mL) were grown for 3 h at 37 °C and then treated with 5 mM H_2O_2 or an equivalent volume of ddH_2O for an additional 3 h at 37 °C prior to the enumeration of CFU.

In vitro growth assays

Overnight cultures of WT, Δ*egtV*, and Δ*egtV::egtV H. pylori* PMSS1 were grown for 16–18 h at 37 °C, diluted to OD_{600} 0.01 in fresh medium, and grown for an additional 21 h at 37 °C. CFU were measured immediately after subculturing (t=0) and again after 4, 8, or 21 h of growth. For coculture assays, overnight cultures of WT, Δ*egtV*, and Δ*egtV::egtV H. pylori* PMSS1 were diluted to OD_{600} 0.01 in fresh medium and combined pairwise in 1:1 mixtures (final OD_{600} 0.02). CFU were measured immediately after subculturing (t=0) and again after 4, 8, or 21 h of growth. CFU were enumerated on nonselective and chloramphenicol- or kanamycin-containing plates. The total CFU in each coculture were determined using nonselective plates, whereas the CFU of the Δ*egtV* and Δ*egtV::egtV* strains were determined using chloramphenicol- or kanamycin-containing plates, respectively. WT *H. pylori* CFU were determined by subtracting the number of CFU on selective media from the total CFU.

H. pylori infection of human gastric cells

AGS cells were seeded in DMEM supplemented with 10% (v/v) HI-FBS using 100-mm tissue-culture treated plates (Corning) at 10^6 cells per dish. After 3 days, the cell culture medium was replaced with 10 mL fresh medium supplemented with EGT-d^3 (1 μg/mL) or vehicle control (ddH_2O). Following a 24-h incubation, the cells were washed twice with Dulbecco's PBS (DPBS; HyClone) and covered with 10 mL co-culture medium (DMEM supplemented with 10% (v/v) Brucella broth and 5% (v/v) HI-FBS). 1 mL of the co-culture medium was transferred to an Eppendorf tube, cleared by centrifugation (21,000 x *g*, 2 min, room temperature), and the supernatant was stored at –80 °C until further analysis (t=0 h sample, Figure 3D). Exponential-phase liquid cultures of *H. pylori* were pelleted by centrifugation (3,180 x *g*, 5 min, room temperature) and resuspended in Brucella broth supplemented with 10% (v/v) HI-FBS to an OD_{600} of 2. Bacterial resuspensions were added to the AGS cells at a multiplicity of infection (MOI) of 50, and the infected cells were incubated in a humidified 5% CO_2 incubator at 37 °C for 10 h. An equal volume of 10% (v/v) HI-FBS in Brucella broth was used as a mock infection control. After 10 h, 1 mL of conditioned medium from mock- and *H. pylori*-infected cells was transferred to an Eppendorf tube and cleared by centrifugation (21,000 x *g*, 2 min, room temperature). The clarified supernatants were transferred to

Please cite this article in press as: Dumitrescu et al., A microbial transporter of the dietary antioxidant ergothioneine, Cell (2022), https://doi.org/10.1016/j.cell.2022.10.008

fresh tubes and stored at –80 °C until further analysis (Figure 3C; t=10 h sample, Figure 3D). To isolate *H. pylori*, the remaining conditioned medium (~9 mL) from *H. pylori*-infected AGS cell cultures was transferred to a conical tube, AGS cells were washed twice with DPBS, and washes were collected in the same tube. The combined conditioned media and DPBS washes were then centrifuged at low speed (300 x *g*, 3 min, room temperature) to pellet any mammalian cells, and the supernatant was then transferred to a fresh tube and centrifuged again (3,000 x *g*, 5 min, room temperature) to pellet *H. pylori*. Cells were resuspended in 1 mL PBS to measure CFU and were then pelleted (3,000 x *g*, 5 min, room temperature) and stored at –80 °C until further analysis (Figures 3E and 3F). Following the washes, AGS cells were treated with 400 μg/mL kanamycin and 160 μg/mL chloramphenicol in DMEM for 1 h, and then washed again with DPBS. Cells were collected via dissociation by TrypLE Express (Gibco) and pelleted by centrifugation (300 x *g*, 3 min, room temperature in 15-mL conical tubes (Corning); then 21,000 x *g*, 2 min, room temperature in Eppendorf tubes), and then resuspended in PBS for enumeration via the Trypan Blue (Thermo) exclusion test using a Countess II FL automated cell counter (Applied Biosystems). Then cells were pelleted (21,000 x *g*, 2 min, room temperature) and stored at –80 °C until further analysis (Figure 3B).

Mouse infections

For single infections, ten mice per time point (1, 8, or 16 weeks) were orally infected with 10^8 CFU of mid-exponential-phase cultures of *H. pylori* PMSS1 WT, Δ*egtV*, or Δ*egtV::egtV*, and five mice were mock-infected with media alone. For competition experiments, eight mice per group were infected for 2 weeks with equal mixtures of WT and Δ*egtV* or Δ*egtV* and Δ*egtV::egtV H. pylori* PMSS1 for a total of 10^8 CFU per animal. Mice were euthanized by CO_2 asphyxiation followed by cervical dislocation at 1-, 2-, 8-, or 16-weeks post-infection. After removal of the forestomach, the remaining stomach tissue was dissected, weighed, and homogenized in Brucella broth using a bead beater (BioSpec) prior to measuring CFU. For single infections, the stomach was dissected into two pieces: one half for CFU determination, and one half for histopathologic analysis.

Measurement of EGT in mouse gastric tissue

To measure the EGT content of murine gastric tissue and digested chow isolated from mouse stomachs, six mice were mock-infected with media alone (5 μL DMEM) to mimic infection conditions and then euthanized after two weeks. Mice were dissected, the food content of the stomach was gently scraped and added to a tube containing 1 mL PBS, and then the stomach was washed with PBS and collected in 1 mL PBS. Mouse chow (2018 Teklad Global) was homogenized and the powder (50 mg) was added to a tube containing 1 mL PBS. Samples were supplemented with 1 μg EGT-d^9 and then homogenized using a bead beater. 100 μL of each mixture was added to 400 μL thiol extraction buffer and EGT levels were measured as described before.

Gastric histopathology

Half of the excised stomach (containing the corpus and antrum) from 35 total mice either mock-infected (N=5) or infected with WT, Δ*egtV*, or Δ*egtV::egtV H. pylori* PMSS1 (N=10 mice per condition) for 16 weeks were immersion-fixed for 24 h in 10% neutral-buffered formalin, and then trimmed, transferred to 70% (v/v) ethanol, and submitted for routine processing, embedding, sectioning and staining for hematoxylin and eosin (H&E) to the Histology Service in the Comparative Pathology Research Core (Department of Comparative Medicine, Yale University School of Medicine). The H&E-stained sections of stomachs were examined blind to experimental manipulation and scored by semiquantitative analysis adapted from published methods for edema, inflammation, gland loss, and gland hyperplasia (Montgomery et al., 2007; O'Connor et al., 2009). Severity scores ranged from 0–5 as follows: 0, within normal limits or absent; 1, minimal; 2, mild; 3, moderate; 4, marked; 5, severe. Severity of injury represents the total additive score for each mouse.

Bioinformatic and phylogenetic analyses

Protein domains and functions were predicted using BLASTp, BioCyc, or InterProScan based upon sequence homology to characterized proteins. Prediction of membrane protein topology was performed using the TOPCONS online web server. Protein sequence identities and similarities were calculated using BLASTp. Homologs to the predicted solute-binding portion of HPG27_777 (aa 282–553) were identified using BLASTp (alignment score $\geq$100). Protein sequences were aligned with Promals3D. Geneious Prime 8 was used to align solute-binding domains using global alignment with free end gaps, and then a protein phylogenetic tree was constructed using the neighbor-joining tree building method and Jukes-Cantor genetic distance model. Phylogenetic trees were further customized using iTOL v6.

Human fecal EGT-d^9 metabolism assays

EGT-d^9 metabolism assays were performed under anaerobic conditions (20% CO_2, 10% H_2, and 70% N_2) in a Coy anaerobic chamber. Human fecal samples (100 μL) were mixed with 675 μL buffer (20 mM Tris, pH 7.8) containing 25 μL EGT-d^9 (1 mg/mL stock) or an equal volume of buffer alone and incubated for 24 h at 37 °C. Samples were then spiked with internal standard (1 μg EGT-d^3), and 100 μL of each reaction mixture were mixed with 400 μL thiol extraction buffer to quantify EGT-d^9 by LC–MS, or with 400 μL 95% (v/v)

ACN with 0.1% (v/v) formic acid to quantify TMA-d^9. Samples for the quantification of EGT-d^9 were then treated with mBBr as described above; samples for the quantification of TMA-d^9 were centrifuged (10 min, 21,000 x *g*, room temperature) and the supernatant was removed and stored at 4 °C until LC–MS analysis.

QUANTIFICATION AND STATISTICAL ANALYSIS

All quantitative experiments were performed in technical triplicate and were repeated a minimum of three times unless otherwise specified. Statistical analyses were performed using GraphPad Prism 9.1.2. Details regarding statistical parameters are described in the figure legends.

Supplemental figures

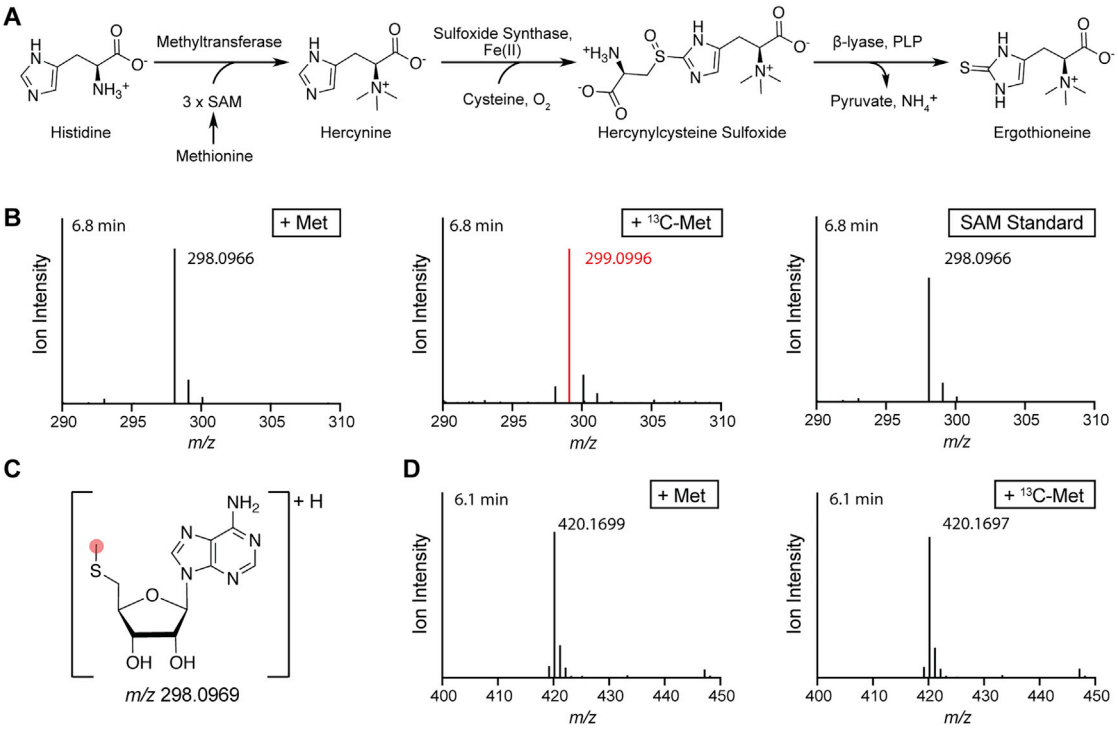

Figure S1. ***H. pylori*** **does not biosynthesize EGT, related to Figure 1**

(A) Abbreviated canonical pathway for EGT biosynthesis in fungi and most bacteria (Seebeck, 2010; Bello et al., 2012).

(B) Cell extracts from *H. pylori* G27MA cultures supplemented with 10 mM methionine (Met) or methionine-(*methyl*-^{13}C) (^{13}C-Met) were labeled with mBBr and analyzed by LC-MS. The total ion chromatogram (TIC) mass spectra at 6.8 min depicting the 5′-methylthioadenosine fragment of SAM derived from Met-treated (left) or ^{13}C-Met-treated (middle) *H. pylori* cultures, or from a SAM standard (right).

(C) Chemical structure of the 5′-methylthioadenosine fragment of SAM. The position labeled via ^{13}C-Met incorporation is highlighted in red.

(D) TIC mass spectra at 6.1 min depicting the mB-EGT adduct from Met-treated (left) or ^{13}C-Met-treated (right) *H. pylori* extracts.

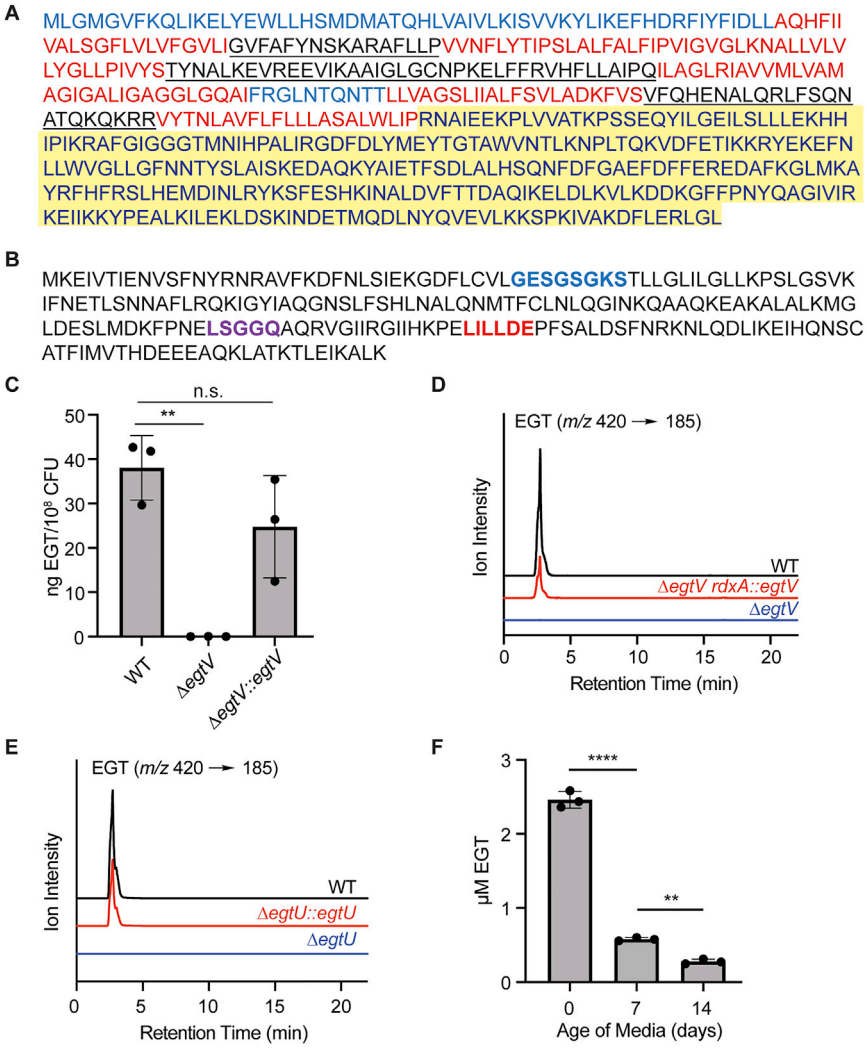

Figure S2. *H. pylori HPG27_777* (*egtU*) and *HPG27_778* (*egtV*) are required for EGT uptake, related to Figure 2

(A and B) The amino-acid sequences of (A) HPG27_777 and (B) HPG27_778 are shown. Predicted periplasm-exposed residues in (A) are shown in blue, cytosolic residues are underlined, and transmembrane helices are shown in red. The region comprising the predicted periplasmic solute-binding domain is highlighted in yellow. Cytosolic, periplasmic, and transmembrane regions were predicted using the TOPCONS membrane protein topology web server. ATPase Walker A, Walker B, and signature motifs in (B) are shown in blue, red, and purple, respectively.

(C) The EGT content of WT, Δ*egtV*, and Δ*egtV::egtV H. pylori* PMSS1 cell extracts was quantified by LC-MS analysis following mBBr labeling. **$p < 0.01$; n.s., not significant, by one-way ANOVA with Holm-Šídák's multiple comparisons test. Error bars represent means ± SD of biological replicates.

(D and E) Cell extracts of WT, Δ*egtV*, and Δ*egtV rdxA::egtV* (D) or WT, Δ*egtU*, and Δ*egtU::egtU* (E) *H. pylori* G27MA were treated with mBBr and analyzed by LC-MS. Selected reaction monitoring (SRM) traces of mB-EGT (*m/z* 420 → 185, described in STAR Methods) from each strain are shown.

(F) The EGT content of freshly prepared Brucella broth, the primary component of standard *H. pylori* culture medium, was measured via mBBr labeling and LC-MS analysis after 0, 7, or 14 days. **$p < 0.01$; ****$p < 0.0001$, by one-way ANOVA with Tukey's multiple comparisons test. Error bars represent means ± SD of biological replicates.

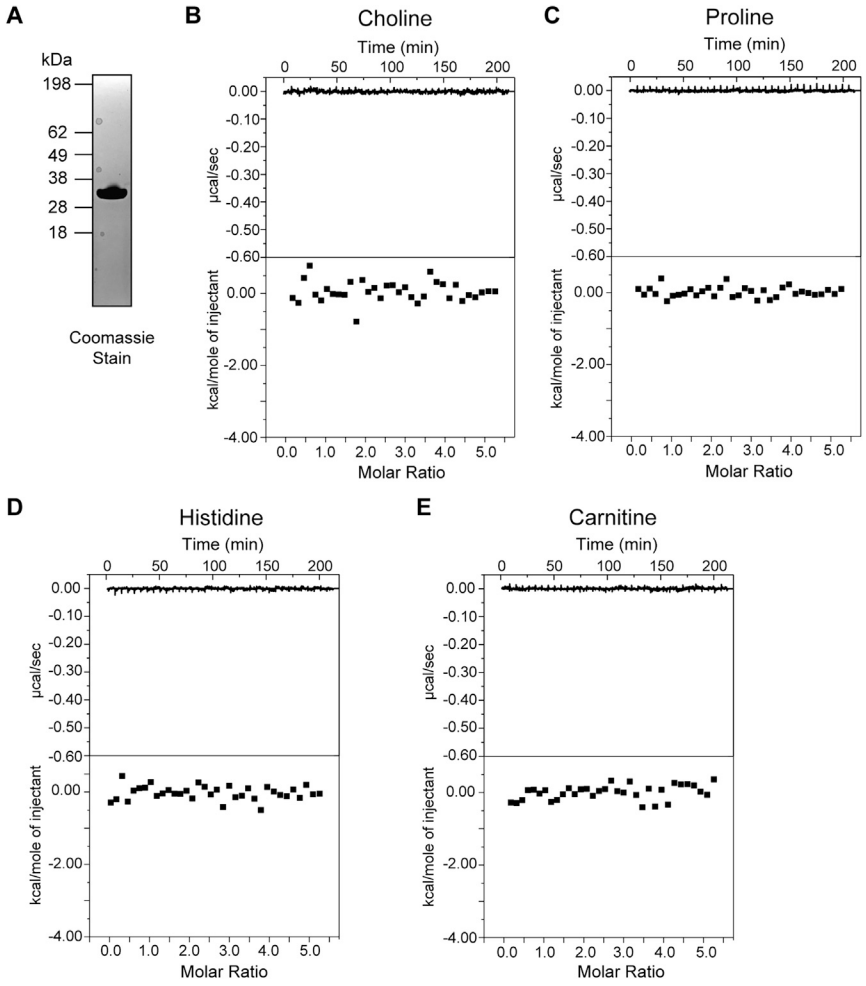

Figure S3. The *H. pylori* EgtU solute-binding domain (SBD) does not bind to choline, proline, histidine, or carnitine, related to Figure 2

(A) The *H. pylori* EgtU SBD (aa 282–553) was heterologously expressed as an N-terminal His_6-fusion protein in *E. coli* and purified to homogeneity using Ni-affinity and size-exclusion chromatography.

(B–E) Binding of the purified EgtU SBD to (B) choline, (C) proline, (D) histidine, and (E) carnitine was measured by ITC. Data are representative of at least 2 independent experiments.

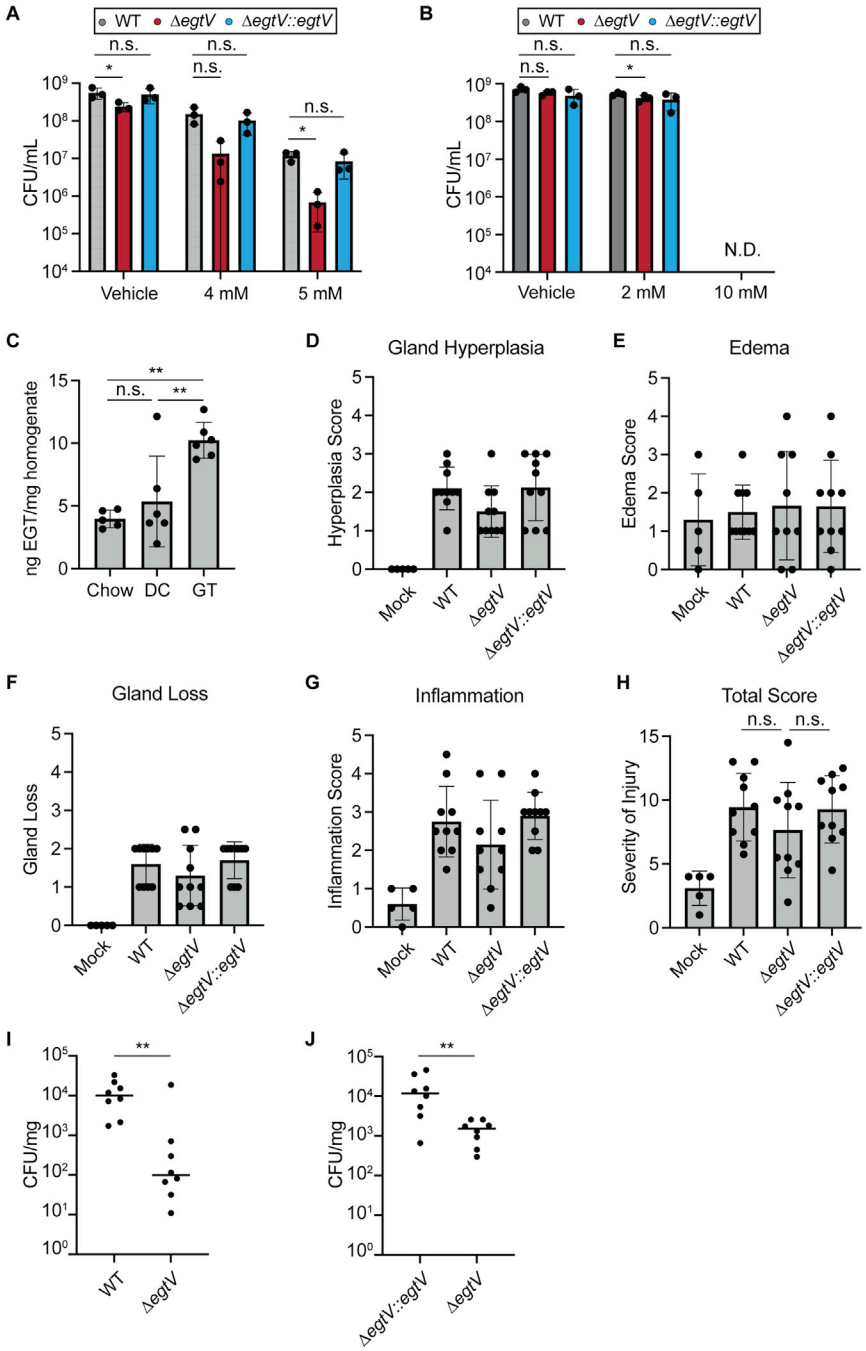

Figure S4. EgtV contributes to the competitive colonization of *H. pylori*-infected mice but does not influence gastric pathology, related to Figure 4

(A and B) CFU of WT, Δ*egtV*, and Δ*egtV::egtV H. pylori* G27MA were enumerated following treatment with the indicated concentrations of bleach for 15 min. Vehicle and 5-mM data from (A) are the same as in Figure 4A. n.d., not detected. *p < 0.05; n.s., not significant, by two-way ANOVA with Fisher's LSD test. Error bars represent means ± SD of biological replicates.

(C) The EGT content of mouse chow, digested chow (DC) isolated from mouse stomachs, and murine gastric tissue (GT) was determined via mBBr-labeling and LC-MS analysis. **p < 0.01; n.s., not significant, by one-way ANOVA with Tukey's multiple comparisons.

(D–H) Formalin-fixed, paraffin-embedded tissue from the stomachs of mice infected with WT, Δ*egtV*, or Δ*egtV::egtV H. pylori* PMSS1 for 16 weeks (N = 10 mice per condition) or mock-infected controls (N = 5 mice) was sectioned and stained with hematoxylin and eosin (H&E). Sections were blinded and scored for gland hyperplasia (D), edema (E), gland loss (F), and inflammation (G). The total score (H) represents the additive score of all injury markers for each mouse. One Δ*egtV* sample was not scored for edema because the anatomical layout could not be determined. n.s., not significant, by one-way ANOVA with Tukey's multiple

(legend continued on next page)

comparisons test. Error bars represent means ± SD. Histopathology analyses were performed twice using mice from two independent experiments with similar results.

(I and J) CFU of WT, Δ*egtV*, and Δ*egtV::egtV H. pylori* in the stomachs of mice co-infected with WT and Δ*egtV* (I) or Δ*egtV::egtV* and Δ*egtV* (J) *H. pylori* PMSS1 for 2 weeks. Horizontal bars denote the median CFU. **$p < 0.01$; n.s., not significant by ratio-paired t test.

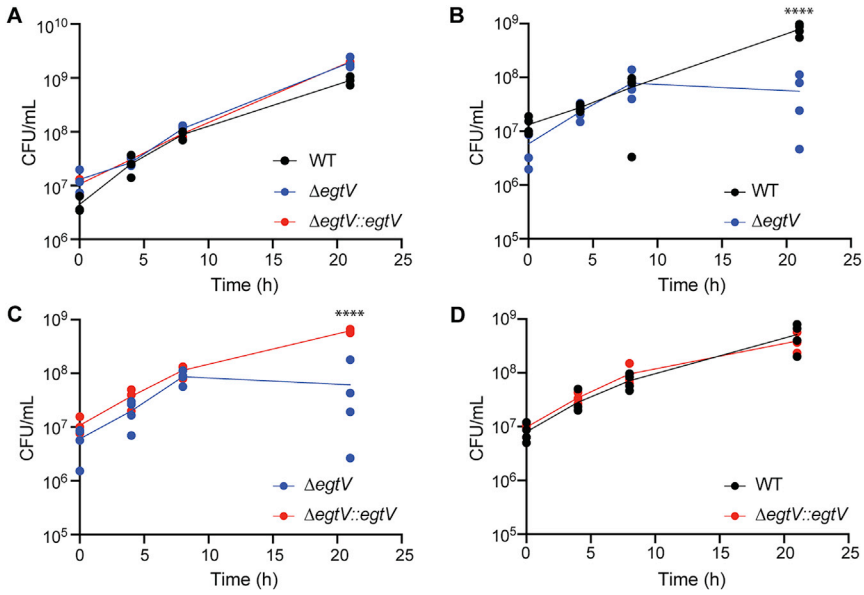

Figure S5. Δ*egtV* is outcompeted by WT and Δ*egtV::egtV in vitro*, related to Figure 4

CFU of WT, Δ*egtV*, and Δ*egtV::egtV H. pylori* PMSS1 strains cultured individually (A) or as 1:1 mixtures (B–D) were enumerated at the indicated time points. ****$p < 0.0001$, by two-way ANOVA with Holm-Šídák's multiple comparisons test. N = 4.

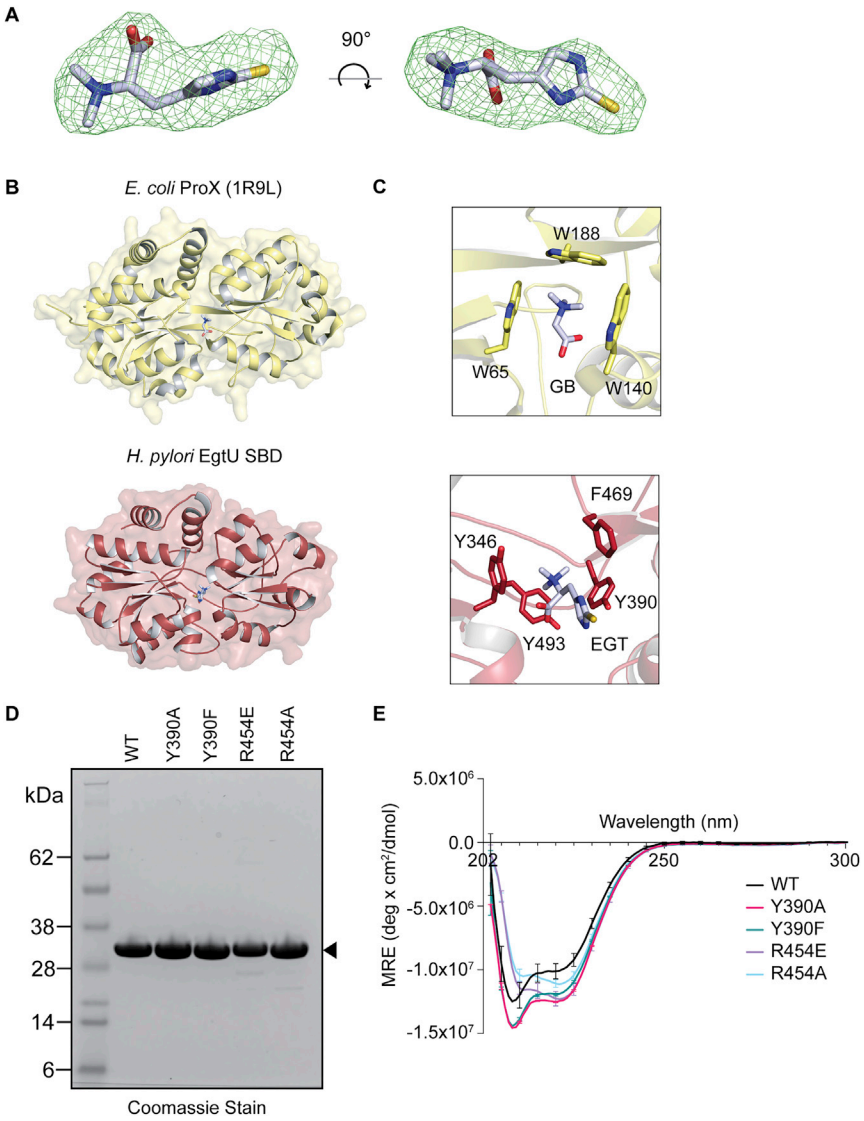

Figure S6. *H. pylori* EgtU SBD is similar in global structure to the glycine betaine-binding protein ProX, related to Figure 6 and Tables S1 and S3

(A) Mesh showing polder map of EGT ligand density, contoured to 5 σ.

(B) Crystal structure of *E. coli* ProX (1R9L) bound to glycine betaine (top) and the *H. pylori* EGT-bound EgtU SBD (bottom). ProX is the solute-binding protein of a glycine betaine ABC transporter that has an overall secondary structure similar to that of the EgtU SBD.

(C) Betaine box residues in *E. coli* ProX surrounding glycine betaine (top) or in the *H. pylori* EgtU SBD surrounding EGT (bottom).

(D) Representative SDS-PAGE of EgtU WT and mutant SBD proteins.

(E) Circular dichroism (CD) spectroscopy analysis of EgtU WT and mutant SBD proteins. CD spectra represent the average of at least two independent experiments. Error bars represent standard deviation.

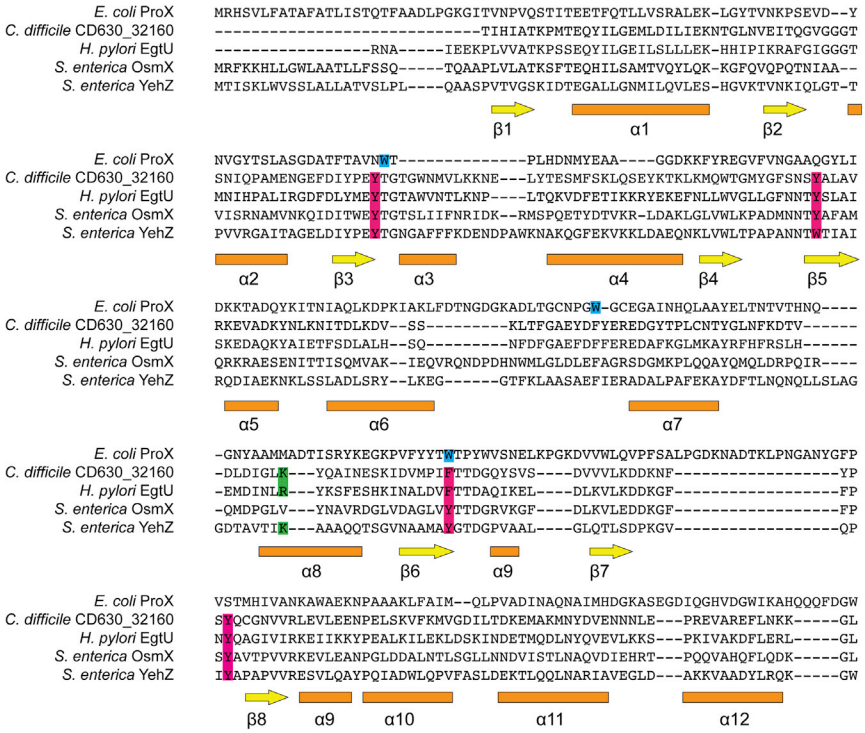

Figure S7. Multiple-sequence alignment of EgtU SBD homologs, related to Figure 6 and Table S2

The SBD sequences of *H. pylori* EgtU, *S. enterica* Typhimurium YehZ and OsmX, *C. difficile* CD630_32160, and the *E. coli* glycine betaine-binding protein ProX were aligned using Promals3D. The betaine-binding residues from *H. pylori* EgtU (Y346, Y390, F469, Y493) are highlighted in pink, while the corresponding residues from the glycine betaine-binding protein ProX are highlighted in blue. R454, which is conserved as a positively charged residue in EGT-transporting proteins, is highlighted in green. Predicted secondary structures (α helices and β strands) conserved in all proteins are indicated.